NAVAL POSTGRADUATE SCHOOL

MONTEREY, CALIFORNIA

THESIS

A VERIFICATION OF OPTICAL DEPTH RETRIEVALS FROM HIGH RESOLUTION SATELLITE IMAGERY

by

Jack Robert Evans

March 2007

Thesis Advisor:	Philip Durkee
Second Reader:	Carlyle Wash

Approved for public release; distribution is unlimited.

THIS PAGE INTENTIONALLY LEFT BLANK

REPORT DOCUMENTATION PAGE		Form Approved OMB No. 0704-0188

1. AGENCY USE ONLY *(Leave blank)*	2. REPORT DATE	3. REPORT TYPE AND DATES COVERED
	March 2007	Master's Thesis

4. TITLE AND SUBTITLE A Verification of Optical Depth Retrievals From High Resolution Satellite Imagery	5. FUNDING NUMBERS
6. AUTHOR(S) Jack R. Evans	
7. PERFORMING ORGANIZATION NAME(S) AND ADDRESS(ES) Naval Postgraduate School Monterey, CA 93943-5000	8. PERFORMING ORGANIZATION REPORT NUMBER
9. SPONSORING /MONITORING AGENCY NAME(S) AND ADDRESS(ES) N/A	10. SPONSORING/MONITORING AGENCY REPORT NUMBER

11. SUPPLEMENTARY NOTES The views expressed in this thesis are those of the author and do not reflect the official policy or position of the Department of Defense or the U.S. Government.

12a. DISTRIBUTION / AVAILABILITY STATEMENT	12b. DISTRIBUTION CODE
Approved for public release; distribution is unlimited	

13. ABSTRACT (maximum 200 words)

A new technique has been developed using high resolution satellite imagery to derive aerosol optical depths by measuring the difference of the radiances inside and outside of shaded regions Vincent (2006). This approach has shown promise as a new means of providing aerosol optical depth in regions that have proven difficult using more traditional means. Initial studies have been done primarily over desert/arid environments with some limited work over urban regions. This thesis takes the next step by focusing on the challenges that come along with using this technique in an urban environment and by exploring the relationship of how this technique is affected by different surface types. Four different surface types were examined, dirt, grass, pavement, and "other" which includes a random sampling of surfaces that are commonly found in urban environments. Three of these surface types act remarkably similar while grass surfaces deviate from the results seen with the other surfaces. Results from all the surfaces show a low bias which was not seen in the earlier study. This low bias can possibly be attributed to the aerosol model used when running the Shadow Method program, urban effects.

14. SUBJECT TERMS Aerosol, Satellite Observations, Aerosol Optical Depth Retrieval, Shadow, Shadow Method, High-Resolution Commercial Satellite Imagery, QuickBird, Dirt, Grass, Pavement, Urban,	15. NUMBER OF PAGES 95
	16. PRICE CODE

17. SECURITY CLASSIFICATION OF REPORT	18. SECURITY CLASSIFICATION OF THIS PAGE	19. SECURITY CLASSIFICATION OF ABSTRACT	20. LIMITATION OF ABSTRACT
Unclassified	Unclassified	Unclassified	UL

NSN 7540-01-280-5500 Standard Form 298 (Rev. 2-89)
Prescribed by ANSI Std. 239-18

THIS PAGE INTENTIONALLY LEFT BLANK

Approved for public release; distribution is unlimited.

A VERIFICATION OF OPTICAL DEPTH RETRIEVALS FROM HIGH RESOLUTION SATELLITE IMAGERY

Jack R. Evans
Captain, United States Air Force
B.S., Texas A&M University, 1998

Submitted in partial fulfillment of the
requirements for the degree of

MASTER OF SCIENCE IN METEOROLOGY

from the

NAVAL POSTGRADUATE SCHOOL
March 2007

Author: Jack R. Evans

Approved by: Philip A. Durkee
Thesis Advisor

Carlyle Wash
Second Reader

Philip A. Durkee
Chairman, Department of Meteorology

THIS PAGE INTENTIONALLY LEFT BLANK

ABSTRACT

A new technique has been developed using high resolution satellite imagery to derive aerosol optical depths by measuring the difference of the radiances inside and outside of shaded regions Vincent (2006). This approach has shown promise as a new means of providing aerosol optical depth in regions that have proven difficult using more traditional means. Initial studies have been done primarily over desert/arid environments with some limited work over urban regions. This thesis takes the next step by focusing on the challenges that come along with using this technique in an urban environment and by exploring the relationship of how this technique is affected by different surface types. Four different surface types were examined, dirt, grass, pavement, and "other" which includes a random sampling of surfaces that are commonly found in urban environments. Three of these surface types act remarkably similar while grass surfaces deviate from the results seen with the other surfaces. Results from all the surfaces show a low bias which was not seen in the earlier study. This low bias can possibly be attributed to the aerosol model used when running the Shadow Method program, urban effects.

THIS PAGE INTENTIONALLY LEFT BLANK

TABLE OF CONTENTS

LIST OF FIGURES

LIST OF TABLES

THIS PAGE INTENTIONALLY LEFT BLANK

ACKNOWLEDGMENTS

I would like to thank my thesis advisor Prof. Philip A. Durkee who not only guided me through the thesis research but provided the inspiration for this work. I would also like to thank Kurt Nielsen who on a regular basis acted as a sounding board for the ideas and concepts that went into this thesis.

Thanks must also go to Ryan Dombrock whose parallel research and automation methods enabled me to accomplish more work than I would have been able to accomplish with the then current data processing methods.

I thank LCDR Vincent for the initial work that was done on this subject area. This visionary approach to an old problem provided me with the means to carry on my education.

Finally I thank my fellow master's students for their camaraderie and friendship.

THIS PAGE INTENTIONALLY LEFT BLANK

I. INTRODUCTION

The Earth's atmosphere is composed of material to include gaseous molecules, liquids, and solids (aerosols). Aerosols will be the focus of this thesis. Aerosols can come in many forms both natural and anthropogenic. Some of the natural sources include volcanic activity, forest and prairie fires, the earth's surface (i.e. sand and dust storms), especially in desert/arid regions, vegetation (i.e. the blue haze often observed over forested regions), and finally the ocean. Anthropogenic sources fall under three categories; industrial sources, energy utilities, and personal sources. Industrial sources come from manufacturing of products from raw materials such as iron from ore, lumber from trees, gasoline from crude oil, and stone from quarries. It also comes from the conversion of raw materials to products such as automobile bodies from steel, furniture from lumber, paint from solids and solvents, and asphalt paving from rock and oil. The majority of particulates from energy-producing utilities come from the production of electricity. Personal sources mostly revolve around combustion of some form or another. The typical personal sources are automobiles, home furnaces, home fireplaces and stoves, backyard grills and the open burning of refuse and leaves. The typical U.S. family of four is estimated to contribute 72 kilograms of particulate matter into the atmosphere per year (Boubel, et. al. 1994).

The battlefield environment can also act as a major or local source. Activity such as bombing can eject significant amounts of material into the atmosphere, burning of damaged buildings or vehicles, nuclear biological and chemical (NBC) attacks, purposeful smoke screening, and even the passage of vehicles or convoys have the potential to dramatically affect the aerosol distribution in the atmosphere. Although this list does not cover all the sources, it does comprise the majority of natural and anthropogenic sources. This material that enters the atmosphere acts to change the ability of the atmosphere to propagate electromagnetic waves. The measurement of the affect that these aerosols have on the atmosphere is known as the atmosphere's aerosol optical depth (AOD).

The concentration and distribution of aerosols throughout the atmosphere can have several environmental impacts. The global radiative energy budget is one of the most significant. These aerosols act to increase the albedo of the atmosphere thereby decreasing the amount of solar energy reaching the earth's surface. This has implications with respect to off-setting global warming:

> "The ratio of ground-level solar intensity at 0.5μm to extraterrestrial solar intensity can be as high as 0.5 in clean atmospheres but can drop to 0.2-0.3 in polluted areas, indicating that ground-level solar intensity can be decreased as much as 50% by pollution in the air." Also, "increased particulate matter, which decreases visibility and inhibits incoming solar radiation, and increased gaseous pollutant concentrations, which absorb long-wave radiation and increase surface temperatures." (Boubel, et. al. 1994).

The decrease in incoming solar radiation and increase in the trapping of long-wave radiation can be complicated and has an affect on the atmosphere that is not completely understood.

Another impact is on cloud formation, and ultimately precipitation that requires condensation nuclei to start the process. Aerosols either natural or anthropogenic serve as a source for these condensation nuclei. However, it is not as simple as more nuclei producing a greater chance of precipitation.

> A study conducted in St. Louis, Missouri (the Metropolitan Meteorological Experiment, or METROMEX), indicated that the average annual precipitation down wind from this city increased by about 10 percent. These increases closely followed industrial development upwind. This study also demonstrated that precipitation amounts were significantly greater on weekdays (when pollution emissions were higher) than on weekends (when pollution emissions were lower). Corroborative findings have been reported for Paris, France, and for other cities as well. However in areas with insufficient humidity to support the formation of cloud and

> precipitation, studies suggest that the rate of precipitation may actually decrease as pollutant particles (nuclei) compete for available moisture-similar to the effect of over seeding a cloud. (Ahrens 1994).

Fog formation can also be influenced by aerosols in the atmosphere since, just like in precipitation cases, particulates act as condensation nuclei. An increase in these particles especially in urban environments can lead to dense persistent fog. This is very dependent on humidity and the local moisture sources (Boubel, Fox, Turner, and Stern 1994).

From a military standpoint AOD also can play a significant role. The effect that AOD has on visibilities both in the vertical and horizontal can have wide reaching impacts. The first and most obvious is the ability to see or identify the enemy on the battle field. A decrease in visibility is also something that can be used to your advantage to hide from the enemy. Changes in optical depth also impact reconnaissance from both satellites and airborne assets. Targeting sensor effectiveness can be greatly reduced under poor conditions. Flight operations can become hazardous or brought to a standstill when visibilities fall. Airborne particulates have the potential to block targeting lasers or even affect future high energy weapon systems.

Having the ability to properly quantify AOD and its affects on the battlefield and the weapon systems would allow military leaders to tilt these conditions in their favor. This however, is not a simple task. The majority of the time, location-specific observations are not available. Because of this, the use of remote sensing is the most logical tool for trying to retrieve this information. Previous attempts have shown some success but still have some restrictions. These restrictions include the inability to resolve a scene at a high enough resolution to meet the needs of operations. In other cases, the inability to make successful retrievals over highly reflective surfaces such as desert regions severely limits the areas where commanders can take advantage of this type of intelligence. Also, lack of temporal resolution can specifically affect time sensitive operations. These early methods and limitations will be discussed in the Chapter II.

Recently there has been a new approach taken to circumvent the previously mentioned deficiencies. This method known as the Shadow Method recently developed by Vincent (2006) uses advances in remote sensing technology to attempt to retrieve AOD information in a manner that has the potential to be timely, accurate, and capable of being used over highly reflective surfaces. The Shadow Method capitalizes on the capability of high resolution satellites to resolve shadows produced by surface structures. By measuring the radiance values within and outside of a shadow an assessment can be made about the aerosols in the atmosphere. Initial work has shown great promise for this technique. This thesis will validate and expand on Vincent's work toward an eventual goal of operational use.

II. BACKGROUND

A. RELATED RESEARCH

1. Contrast Reduction Method

The Contrast Reduction Method was one of the earliest attempts to resolve atmospheric AOD using a remote sensing platform. The basis of this method relied on the comparison of radiances between surfaces with differing albedo. Through the use of a "contrast transmission function" that relied on optical depth, mean surface reflectance, sun-sensor geometry and a specific aerosol model the AOD could in theory be retrieved. The first attempt with this method was applied over an area with uniform surface properties. This attempt provided marginal results. Kaufman and Joseph (1982) later used surface areas with a higher information content. This "Two Halves" method capitalized on the greater information provided in areas with differing albedo, for example a sea coast. This proved to be a more accurate way of retrieving AODs. However, such areas as sea or lake shores, river banks or forest edges are not prevalent enough to give the desired spatial coverage. Eventually the method was developed by using the variance in histograms of the surface reflections or "Visible Variance method" (Tanre et al 1988). These different attempts at the contrast reduction method all relied on assumed single scattering albedo, aerosol phase function, and surface reflectivity and contrast. This method proved to be highly sensitive to assumptions in the aerosol model and small errors in the single scattering albedo results in large surface albedo errors. In addition, land albedo is not known with certainty since nonuniformity of the land causes error in the resulting optical thickness calculations (Kaufman and Joseph 1982). Over the ocean, changes in wind speed affect the sun-glint pattern and the amount of foam on the sea surface, thereby changing the albedo and introducing errors in optical depth calculations (Kaufman and Joseph 1982).

2. Dark Object Method

The Dark object method is conceptually the simplest method for retrieving aerosols from a remote sensing platform. This approach focuses on areas that have a low surface reflectance such as vegetated regions or areas with dark soils. Any radiance

measured beyond the assumed surface albedo is attributed to scatter from atmospheric aerosols. Like the contrast reduction method the dark object method relies heavily on assumed aerosol models and an assumed surface albedo. These assumptions can lead to significant errors. An error of $\Delta\tau = \pm 0.05$ to ± 0.1 is expected for small optical thickness and increasing to 20-30% for high optical thickness" Kaufman et al (1997).

Another weakness of this method is that it tends to break down over areas of higher surface reflectance such as arid regions and urban areas. In these areas, the background surface reflectance overwhelms scatter from atmospheric aerosols.

One of the problems of the Dark Object method is determining the appropriate backgrounds with a low reflectivity on a global scale. Since aerosols tend to affect the transmittance over vegetated or other dark areas, another means is required to locate appropriate low albedo surfaces. To get around this, an alternative technique using longer wavelengths to determine these areas was formulated. Mid-wave IR is still relatively representative of surface characteristics while not being nearly as sensitive to aerosols. This method proved to be successful for locating pixels that are dark in the visible spectrum. The surface reflectance was still assumed but an investigation of areas where the surface albedo was not well known was possible. Though these wavelengths proved to be relatively insensitive to aerosols they are quite sensitive to suspended dust in the atmosphere. The method breaks down rapidly under those conditions and also has difficulty with areas with high surface reflectance (Kaufman et al. 1997).

In an attempt to get around the high surface reflectance problem Dr. Christina Hsu developed a related method known as "Deep Blue". This method capitalizes on the fact that most bright surfaces are highly reflective in the longer portion of the visible spectrum and not so reflective in the shorter wavelengths such as the part of the spectrum represented by satellite's blue channels. The use of the blue band in combination with other channels infers the properties of the aerosols and can ultimately be used to determine the optical depth. The down side to this approach is that the variability of the optical properties of dust are much greater in the blue region of the spectrum. Also uncertainties from the surface reflectance database, assumptions in the vertical profile and assumptions in the aerosol model can lead to further errors (Hsu et al. 2004).

3. Multi Angle Method

The third method for retrieving aerosol information uses a technique known as the Multi-Angle Method. This method is unique to multi-view sensors such as the Along Track Scanning Radiometer (ATSR-2) and the Multi-angle Imaging Spectro Radiometer (MISR). The ATSR-2 uses a conical scanning mechanism in order to view the same surface location from two different angles. The first scan is taken at a 55° angle ahead of the satellite path and the second scan is taken at nadir. This is demonstrated by Figure 1 (The ATSR Project 2007). MISR uses a different method for obtaining multi-angle scans. It has nine separate cameras with four pointed forward, one pointed nadir, and four pointed aft of the scanning path. This is demonstrated by Figure 2 (JPL 2007).

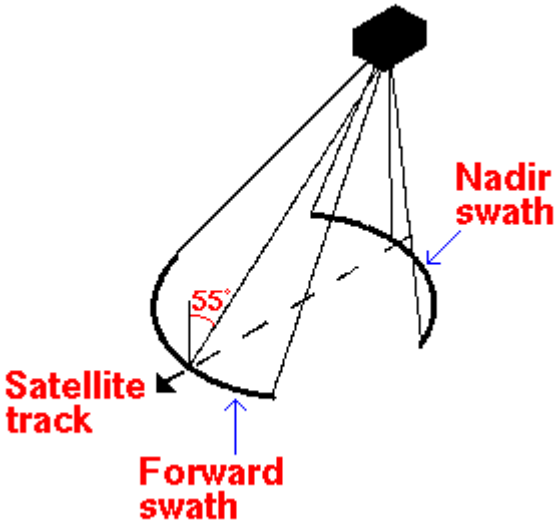

Figure 1. Diagram showing the ATSR along track swath geometry (The ATSR Project 2007)

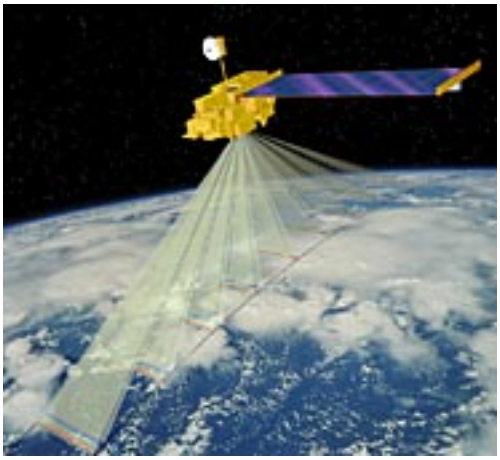

Figure 2. Diagram showing the MISR along track swath geometry (JPL 2007)

The use of radiance values from multiple viewing angles allows for the accurate characterization of surface reflectance while the atmospheric component is modeled for various aerosol types. Moreover, this method succeeds over highly reflective surfaces where the other methods fail. Both Veefkind et al (1998) and Martonchik et al (2004) reported great success with this technique. The primary weakness to this method, however, is that it is highly dependent on multi-view capabilities and modeled aerosols. The MISR has a seven to nine day revisit time which makes it ill-suited to any kind of operational AOD retrievals. There are also known deficiencies in the aerosol models particularly in regards to dust particles (Martonchik et al, 2004).

B. SHADOW METHOD

1. Introduction

Recently there has been an attempt at a new method for retrieving AOD. This method developed by Vincent (2006) is based on new high spatial resolution imagery available through advances in commercial satellites, mainly QuickBird DigitalGlobe (2007). The previous methods discussed, although successful, cannot provide the necessary AOD retrievals over areas of high surface reflectance such as desert regions where there is a multitude of military operations being carried out. The Shadow Method attempts to address this shortfall. This thesis builds on and expands the initial work of Vincent (2006).

2. Shadow Method Summary

As mentioned in the preceding paragraph advances in commercial satellite imagery have seen significant improvements in spatial resolution. With these advancements, we are now capable of resolving detail to include shadows that are produced by manmade structures. A comparison of the radiance values both inside the shadow and the adjacent unshaded regions over a homogeneous surface can be used to extract information about the aerosols contained in the atmosphere.

To extract this information one must first understand the sources or paths of the radiation arriving at the sensor. There are three paths that we are concerned with; direct transmission, diffuse transmission, and diffuse reflection Vincent (2006). Direct transmission is the radiation that travels from the source and is directly reflected into the sensor. Diffuse transmission is the radiation that is scattered off of atmospheric constituents, down to the reflecting surface and then to the sensor. Diffuse reflection is the radiation that is scattered by the atmospheric constituents down to the reflecting surface, back to the atmospheric constituents, back down to the reflecting surface and finally up to the sensor. Figure 3 illustrates these radiative paths. In an unshaded area all three paths for the radiation will be present. In a shaded area or shadow there will be only the diffuse transmission and the diffuse reflection paths. Since both the shaded and unshaded areas presumably have the same diffuse transmission and diffuse reflection; the only difference in the radiance values should be due to the direct transmission. Knowing this should allow us to extrapolate the amount of radiance that is being scattered into the shaded region and therefore retrieve the optical depth.

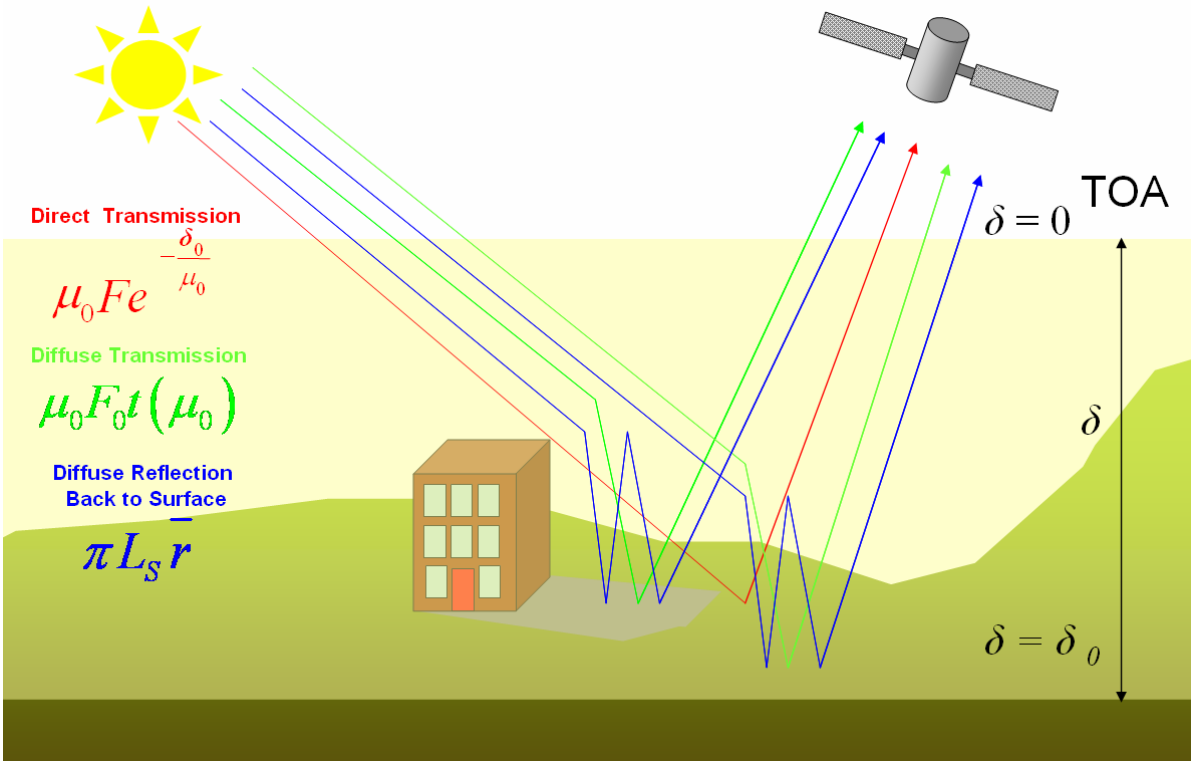

Figure 3. The shadow method uses the difference between the radiances within and outside of the shadowed area to quantify the direct transmission and the total optical depth. Optical depth is defined as the sum of extinction above a vertical position in the atmosphere (therefore equals zero at the top of the atmosphere). Vincent 2006

3. Governing Equation

To make the actual calculations, the individual flux densities must be calculated. Vincent (2006) worked through each individual component and carried it through until he derived a single equation representing the optical depth. A summary of this derivation follows.

The first step is to isolate the three downward flux densities. The direct transmission component can be shown as,

$$\mu_0 F_0 e^{-\delta_0/\mu_0}$$

Where μ_0 is the cosine of the solar zenith angle, F_0 is the spectral solar radiant flux density or irradiance, and δ_0 is the optical depth of the atmosphere.

The diffuse transmission can be shown as,

$$\mu_0 F_0 t(\delta_0, \mu_0)$$

Where t is the transmittance.

The diffuse reflection can be shown as,

$$\pi L_s \bar{r}$$

where L_s is the surface radiance, and $\bar{r}$ is the mean aerosol reflectance.

Now the total flux density can be represented by,

$$\pi L_s = r_s \left(\mu_0 F_0 e^{-\delta_0/\mu_0} + \mu_0 F_0 t(\delta_0, \mu_0) + \pi L_s \bar{r} \right)$$

Solving for L_s which represents the surface intensity or radiance provides,

$$L_s = \frac{r_s}{1 - r_s \bar{r}} \frac{\mu_0 F_0}{\pi} \left(e^{-\delta_0/\mu_0} + t(\delta_{0,} \mu_0) \right)$$

When viewed from a satellite the radiance passes through the atmosphere again and under goes attenuation again. After accounting for optical depth of the atmosphere L_s as viewed from the satellite becomes,

$$L_s = \left[\frac{r_s}{1 - r_s \bar{r}} \frac{\mu_0 F_0}{\pi} \left(e^{-\delta_0/\mu_0} + t(\delta_{0,} \mu_0) \right) \right] e^{-\delta_0/\mu} .$$

The additional extinction is dependent on the sensor viewing angle or μ which represents the cosine of the viewing or sensor zenith angle. This equation represents an unshaded region.

If we want the radiance in a shaded area we need to solve for L_s with out the direct transmittance term. Doing so gives us,

$$L_s^{shaded} = \left[\frac{r_s}{1 - r_s \bar{r}} \frac{\mu_0 F_0}{\pi} t(\delta_{0,} \mu_0) \right] e^{-\delta_0 / \mu}$$

By subtracting the shaded region from the unshaded region we can simplify the equation into something that can be used with our measurements. The equation becomes,

$$L_s^{unshaded} - L_s^{shaded} = L_d = \frac{r_s}{1 - r_s \bar{r}} \frac{\mu_0 F_0}{\pi} e^{-\delta_0 \left(\frac{1}{\mu_0} + \frac{1}{\mu} \right)}$$

Then solving for the total optical depth, δ_0 we get

$$\delta_0 = \left(\frac{\mu_0 \mu}{\mu + \mu_0} \right) \ln \left[\left(\frac{r_s}{1 - r_s \bar{r}} \right) \left(\frac{\mu_0 F_0}{\pi L_d} \right) \right].$$

This equation is now the governing equation to solve for optical depth using the measured difference between the shaded and unshaded regions in an image.

Everything is either known or measured on the right hand side of the governing equation except for the mean aerosol reflectance $\bar{r}$. Vincent assumes that the mean aerosol reflectance is much less than the surface reflectance. He uses the top of the atmosphere (TOA) reflectance initially for his surface reflectance calculations. The total optical depth is retrieved and is then used to determine the mean aerosol reflectance.

Two factors that can have potential impacts on the calculations are molecular Rayleigh scattering and molecular absorption. Vincent (2006) accounts for the Rayleigh scattering by calculating the Rayleigh optical depth for the Quickbird channels based on the work of Russell et al (1993) and Frolich and Shaw (1980). The adjustments are included in Table 1.

Table 1. Molecular Rayleigh optical depths for each of the QuickBird channels based on Eq. (35) assuming a radiometer height of 0 kilometers and atmospheric pressure of 1013.25 hPa. (Vincent 2006)

Band	**Center Effective Wavelenth (micrometers)**	**Molecular Rayleigh Optical Depth**
Panchromatic	0.673	0.05
Blue	0.482	0.17
Green	0.556	0.09
Red	0.658	0.05
Near-Infrared	0.816	0.02

The Quickbird channels have been chosen in a way to avoid or minimize the impact of molecular absorption. This can be seen in Figure 4. Due to this, molecular absorption is assumed to be negligible.

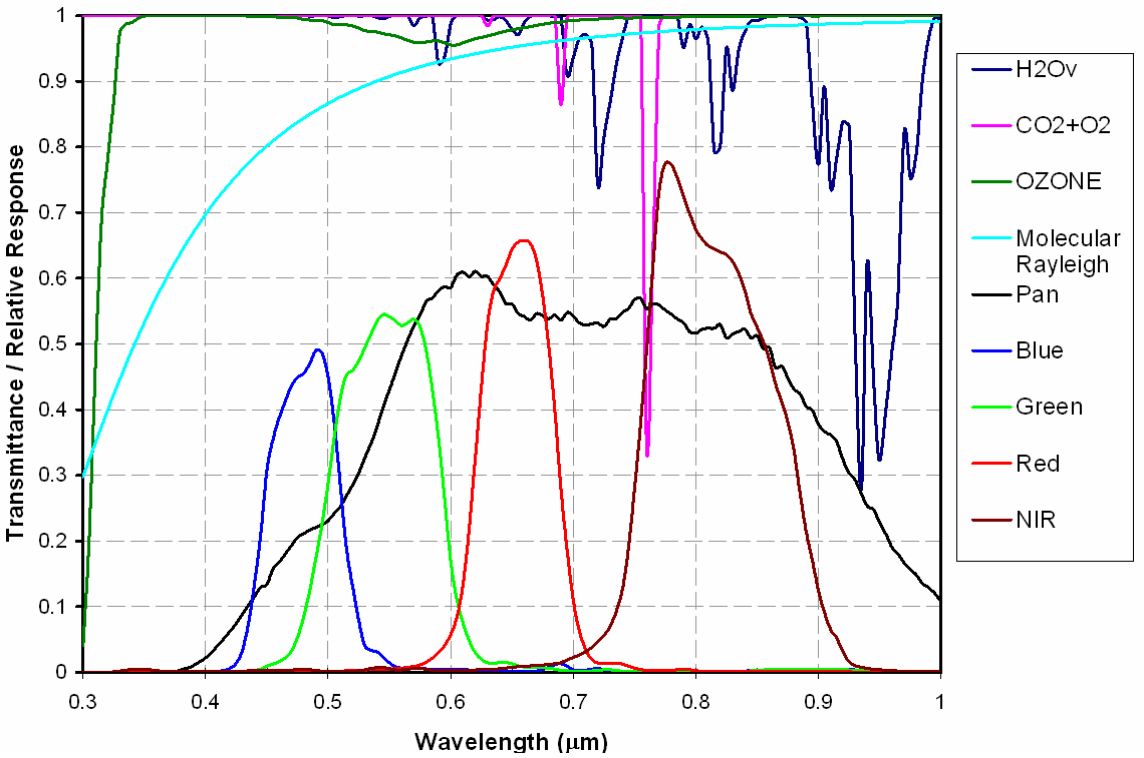

Figure 4. Atmospheric transmittance for water vapor, carbon dioxide, oxygen, ozone and molecular Rayleigh scattering based on a mid-latitude, summer atmosphere as compared to the relative spectral response functions for the each of the QuickBird channels (after Digital Globe 2005a) (Vincent 2006)

III. DATA AND METHODOLOGY

A. DATA

1. Quickbird

Quickbird imagery collected by DigitalGlobe and ordered through the Commercial Satellite Imagery Library (CSIL) was chosen for its unique ability to provide high-resolution imagery not capable by any other current commercial satellite. Imagery is provided in an 11-bit, un-rectified NITF 2.0 format on a DVD (Vincent 2006). Quickbird flies at an altitude of 450 km with a 98 degree sun-synchronous inclination. The revisit interval is 1-3.5 days depending on the latitude at 0.6 meter resolution and has a period of 93.4 minutes. The overpass time is 1030 local at the equator. The nominal swath width is 16.5 km at nadir. A typical single area image is 16.5 km by 16.5km but it is capable of retrieving a strip image of 16.5 km by 165 km. The images used in this thesis, however, consisted of four different scans that when combined provided an area covering approximately 20 by 17km. Quickbird is capable of both in-track and cross-track viewing angles of up to 30 degrees off nadir. It can retrieve up to 128 gigabits (approximately 57 single images) per orbit. Images can be retrieved in both panchromatic and multispectral modes. Panchromatic resolution is 60 cm at nadir with a bandwidth from 445 to 900 nm. Multispectral resolution is 2.4 m in blue, green, red, and near infrared (NIR) channels, with the blue channel between 450 to 520nm, the green channel between 520 to 600nm, and the red channel between 630 to 690nm, and NIR between 760 to 900nm. The dynamic range is 11 bits per pixel. These characteristics make Quickbird ideal for the application of the Shadow method (DigitalGlobe 2007).

2. AERONET

To determine the validity of the AOD retrievals for the Shadow Method, the Aerosol Robotic Network (AERONET) was used for ground truth. The AERONET program is a global network of sun-photometers operated by NASA and LOA-PHOTON (CNRS) that provides observations of spectral AOD, inversion products, and precipitable water in diverse aerosol regimes. The data is provided in three different quality levels: Level 1.0 (unscreened), Level 1.5 (cloud-screened), and Level 2.0 (cloud-screened and

quality-assured). The measurements are made in eight spectral bands at center wavelengths of 340, 380, 440, 500, 675, 870, and 1020nm, with bandwidths of 2, 4, 10, 10, 10, 10, 10, and 10, respectively. The wavelengths applicable for this study were 440, 675, 870, and 1020nm. Attenuation due to Rayleigh scatter, and absorption by ozone and gaseous pollutants is estimated and removed to isolate the aerosol optical depth. Calibration procedures result in an uncertainty level of ± .02 (GSFC 2007).

B. METHOD OF ANALYSIS

All of the imagery preparation, sampling, and much of the analysis was performed using ENVI 4.1. ENVI is a software program run through IDL that is used for visualization and presentation of all types of digital imagery. ENVI's complete image processing package includes an advanced easy-to-use spectral tool, geometric correction, terrain analysis, radar analysis, and raster and vector GIS capabilities. (ITT, 2007)

1. Imagery Choice

The choice of imagery for this study was dependent on many factors. The first and most important was having a day and time corresponding with available AERONET data retrievals. The imagery also had to provide shadows at a distance from the AERONET site that would be representative of the AOD at the AERONET collection site. For the purposes of this study a distance of a half of a degree or approximately 45 km was chosen to be the maximum radial range from the AERONET site (15km was the furthest sample site). The imagery also had to be sufficiently cloud free to insure that there was neither scatter into the sample path by clouds or that clouds blocked the scatter into the sample area by atmospheric constituents. The image chosen for this study was cloud free and therefore was free from the above concerns. Since this study looked at multiple surface types within one scene, a multitude of shadows was needed. An urban environment provided the most likely opportunity to accomplish this. Imagery from Beijing China on 13 September 2003 met this criterion. Figure 5 displays a MODIS

(GSFC 2007) image of eastern China while Figure 6 displays the composite of the four QuickBird images over Beijing that were used in this thesis.

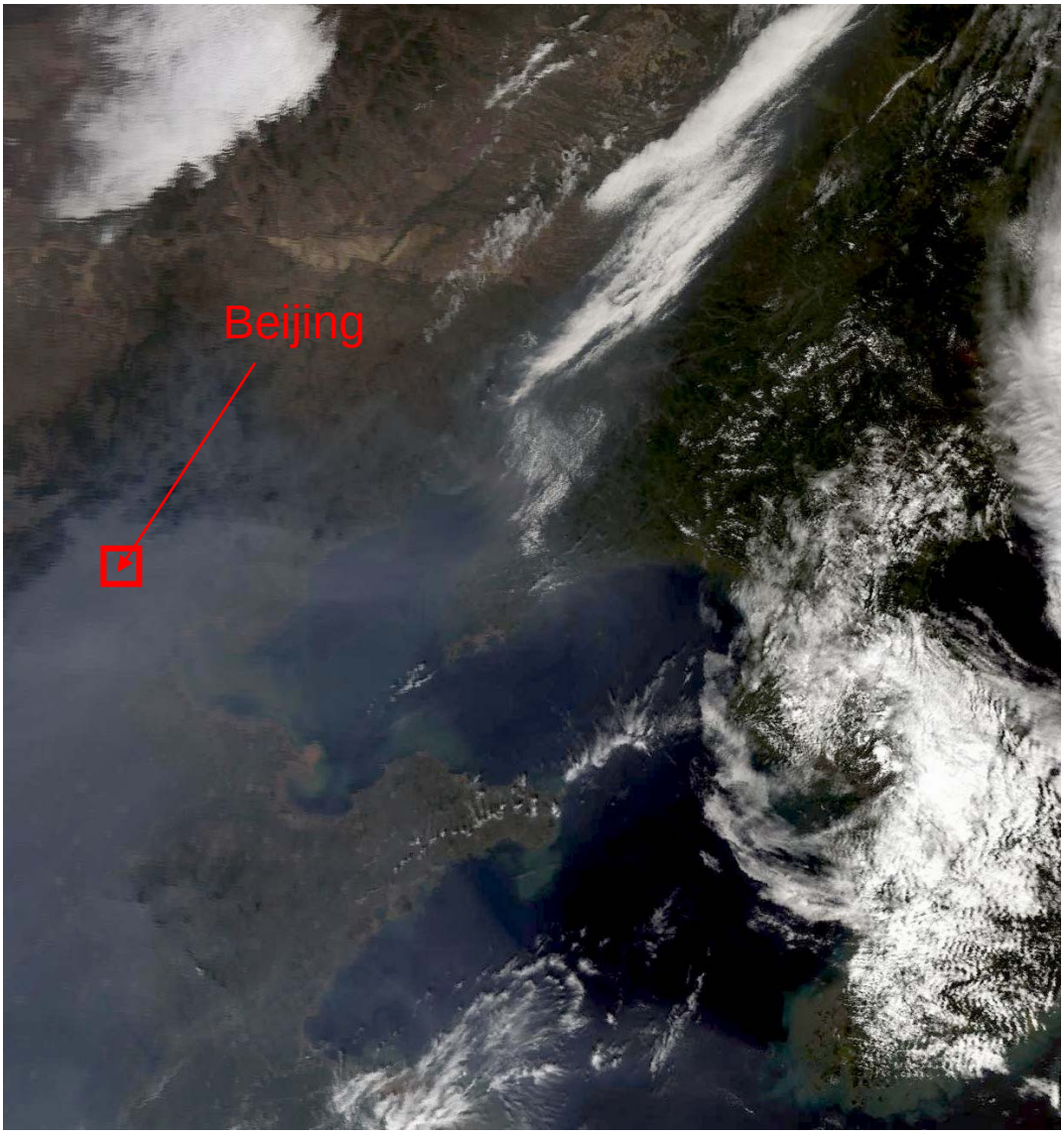

Figure 5. This image is a 250m resolution Modis image of eastern China, 13 September 2003.

Figure 6. This image is a composite of four QuickBird multispectral images located in Beijing China 13 September 2003.

2. Imagery Preparation

a. Image Orthorectification

In order to insure image distortion was accounted for, the images were orthorectified in order to project the image coordinates into real-world coordinates. ENVI provides a built in feature to accomplish this process. ENVI uses a RPC (Rational

Polynomial Coefficients or Rapid Positioning Coordinate) sensor model to orthorectify data from several different platforms including Quickbird. Orthorectification incorporates several sets of input including the image, the RPC model, elevation information and the offset between sea level and the gravitational potential surface or geoid (ITT 2007).

b. Image Conversion to Calibration Absolute Radiance Values

Once the images were orthorectified, they needed to be calibrated for absolute radiance. ENVI provides a tool to perform this calibration; however, Vincent (2006) determined that the ENVI tool that performed this calibration introduced errors that could potentially affect the overall outcome of the AOD calculations. To alleviate this, the Band Math tool within ENVI was used to create an expression that gave an accurate output in watts per meter squared per steradian per nanometer ($W\ cm^{-2}\ sr^{-2}\ nm^{-1}$).

3. ROI Sampling

In order to carry out the Shadow Method paired Region of Interest (ROI) must be selected. The ROI pair consists of a sampling of the radiance values from inside a shadow and a sampling of the radiance values from outside the adjoining shadow over a homogenous surface. An example of this pairing is provided in Figure 7. Seventy-Six ROIs were chosen from the same scene for this thesis. These ROIs were sorted by shadow length and surface type.

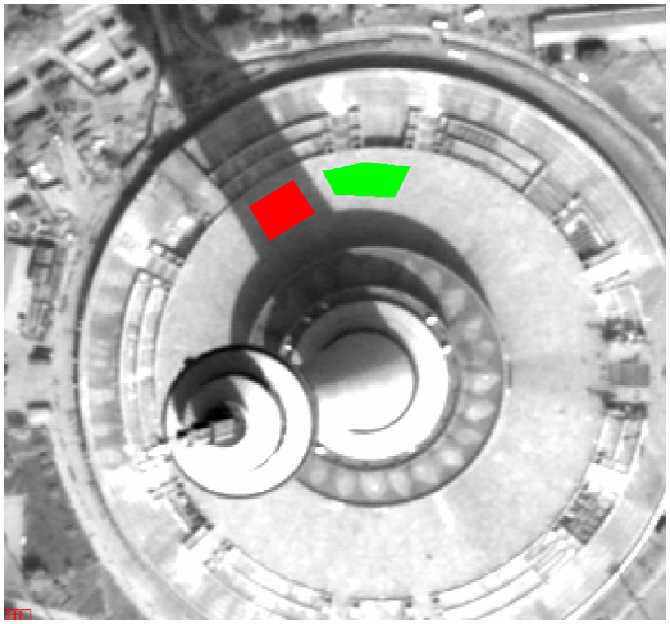

Figure 7. This image is an example of how paired ROIs were taken. The red region is the location where the radiance values were taken for the shaded area in the IDL program and the green region is the location where the radiance values were taken for the unshaded area in the IDL program.

The first analysis investigated shadows by relative length. Long shadows were shadows where a sample of a shadow could be taken without worrying about contamination from edge effects. Edge effects come into play when there is partial pixel filling. Partial pixel filling occurs when there are both shaded and non-shaded regions within a single pixel. In other words, these long shadow ROIs have several pixels between the edge of the sample area and the transition between the shaded and non-shaded region. Invariably, all shadows will be affected by edge effects. Some were short enough that effects were unavoidable. Any shadow that had four or fewer pixels between the apparent base of the shadow casting structure and the apparent edge of the shadow was put into this category. Figure 8 shows an example of a short and long shadow pair. It is noted that ROI samples were taken of matching shadows in the panchromatic images. The shadows that fell under the short category in the multispectral imagery did not fall under the short category, based on the less than four pixel criteria, due to the difference in resolution. This was done in order to maintain a data set in which

a direct comparison could be made across all the channels. Therefore, the short shadows in the panchromatic will not be subject to the same edge effects. This can be seen in Figure 9.

Figure 8. The left image is a 10x zoom example of a shadow that was categorized as a short shadow. It is quite difficult to take a sample without incurring edge effects. The image on the right is a 4x zoom example of a shadow categorized as a long shadow. It is much more likely that a ROI set can be taken with out edge effects being a factor.

Figure 9. The above images, 4x zoom and 1x zoom, represent the short and long shadows respectively in the panchromatic channel and demonstrate that the edge effects are not as apparent in the higher resolution panchromatic imagery.

The second analysis delineated ROIs by surface type. Surface types have varying albedo and therefore varying levels of radiance reflection in the spectral bands. For example vegetative surfaces will reflect higher in the near IR compared to other channels. This difference in the spectral response of the different surfaces has the potential to provide different AOD outputs. With this in mind the ROIs were broken down into four categories: pavement, grass, dirt, and other. The "other" category consisted of a wide assortment of situations such as shadows falling across roof tops, running tracks, and alternately colored parking lots. Examples of the different surfaces types can be seen in Figure 10.

Figure 10. The above images are examples of the four different surface type categories. Starting in the upper left-hand corner and moving clockwise the surface types are grass, dirt, pavement, and other.

4. AOD Extraction

The AOD extraction process involved the use of an IDL program developed by Vincent (2006) and modified by Dombrock (2007). Vincent's original program required five sets of input values: (1) solar and satellite zenith angle, (2) shaded radiance value and standard deviation (retrieved from the ROIs though ENVI), (3) unshaded radiance value and standard deviation (retrieved from the ROIs though ENVI), (4) estimate of single scatter albedo, and (5) estimate of the asymmetry factor. Dombrock (2007) modified the program to directly extract the radiance values from ENVI thereby greatly increasing the speed and efficiency of the AOD calculation process. The modifications to the Shadow AOD program allowed for a much larger sample set to be taken and evaluated.

5. Analysis

The first step in the analysis process was to derive the ground truth. The AERONET channels do not correspond exactly with the Quickbird channels. Therefore, the retrieved AODs had to be extrapolated to the AERONET channel wavelengths. Table 2 provides the effective QuickBird bandwidths and Figure 11 provides the graph with the exponential best-fit curve calculating the AERONET equivalent AOD.

Table 2. QuickBird minimum, maximum and center effective wavelengths (after Digital Globe (2005)) with in band spectral solar irradiance based on Wehrli (1985) spectral solar irradiance curves.

QuickBird Channel	**Minimum Wavelength (nm)**	**Maximum Wavelength (nm)**	**Center Effective Wavelength (nm)**	**Spectral Solar Irradiance (W m^{-2} $nm^{-1)}$**
Ch 1 (Blue)	450	520	482	1973
Ch 2 (Green)	520	600	556	1854
Ch 3 (Red)	630	690	658	1570
Ch 4 (Near-Infrared)	760	900	816	1095
Panchromatic	445	900	673	1506

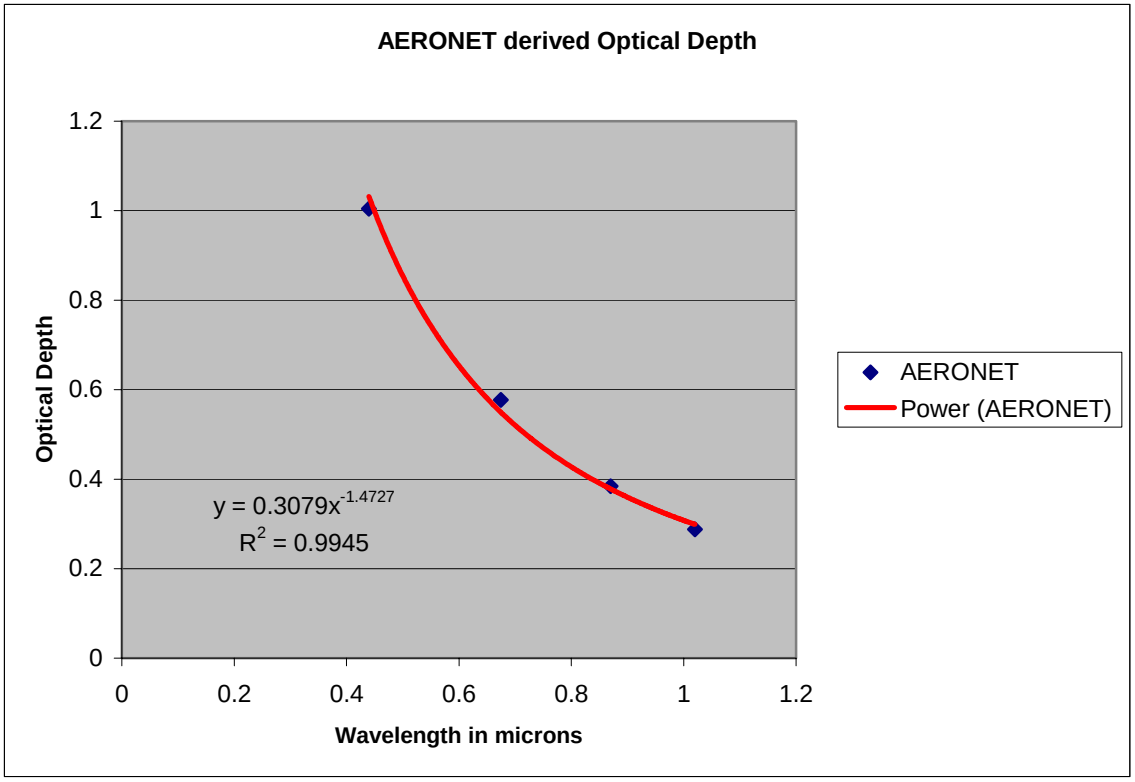

Figure 11. AERONET derived optical depth.

The next step was to compare the Shadow Method AODs with the AERONET derived results. Further information was gathered, including distance of ROIs from the AERONET site, spatial variations of the AOD readings with GIS, and histogram distributions of the results.

In the original Shadow AOD program, the minimum radiance values contained in the shaded portions of the ROIs were used in the calculations to determine the AOD (Vincent 2006). This thesis did a comparison of the ROIs using both the minimum radiance values and the average values within the shaded region. The results are in Chapter IV.

Since this study was located in an urban environment, there are other factors that may contribute to the end results. In an urban environment, there is an increased likelihood of surrounding structures. These surrounding structures can affect the scene in two ways. The first is that they can act as reflectors. The sun lit side of a building can add radiance to a scene both inside and outside of the shaded region. A building can also

act to block part of the sky radiance. This blocking will decrease the amount of aerosol-scattered light into both the shaded and unshaded regions. Figure 12 shows an example of the potential for both affects in the same scene. Buildings one and two act to both block part of the sky radiance and reflect radiance into the ROI produced by building five while buildings three and four act to only block sky radiance into the ROI.

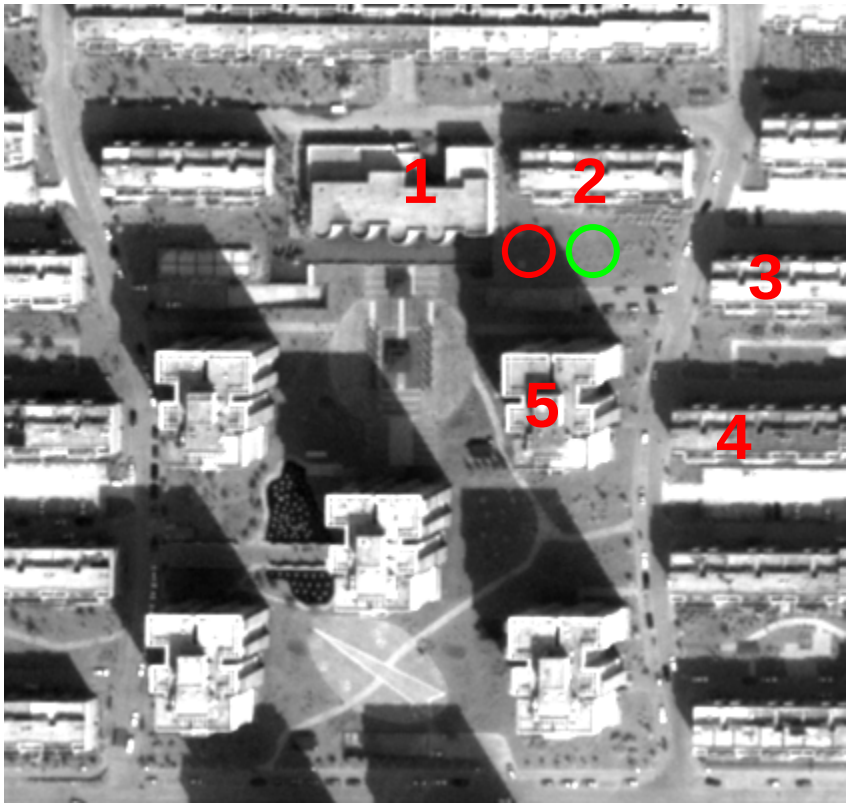

Figure 12. An example of a scene where surrounding buildings can impact the AOD calculations by either reflecting radiance into an ROI or by blocking aerosol scattered radiance into the ROI.

To explore the potential urban impact, ROIs with surrounding buildings and without surrounding buildings were identified. The methodology for determining whether a scene had surrounding building was subjective. Without horizontal measurements and building heights available it was quite difficult to determine the extent of the blocking of the sky radiance or the extent to which added reflectance changed the scene. The buildings were then categorized as either being strong reflectors or not. The

strong reflectors were those buildings that had an illuminated face visible to the ROI while the non-strong reflectors had a shaded face toward the ROI. Regardless of whether the building was a reflector or not they all acted to block part of the sky radiance from aerosol and molecular scatter.

IV. RESULTS

A. GROUND TRUTH

As stated earlier in Chapter III, AERONET was used as ground truth in order to determine the accuracy of the Shadow Method. Since the QuickBird channels do not match the AERONET channels the equivalent channels had to be derived (see Figure 8). After integrating for the QuickBird band widths the AODs for the QuickBird channels were derived and can be seen in Table 3.

Table 3. AERONET integrated (AOD). Derived AERONET AOD values matching QuickBird channels and spectral response.

Channel	Blue	Green	Red	NIR	Panchromatic
Band (microns)	.445-.520	.520-.605	.635-.690	.760-.900	.445-.900
AOD	0.8860	0.7154	0.5659	0.4097	0.5577

B. MIN VS. MEAN COMPARISON

One of the early considerations when running the Shadow Method AOD program developed by Vincent (2006) was the question of the radiance values to be used in the shaded regions. In the unshaded regions the mean value was used for the radiance input while the minimum value or pixel was used in the shaded region. The thought process behind this was that the minimum value would most accurately portray the shaded region and remove, to some extent, any influence of edge effects or contamination by surface variations. This would be particularly important in situations with short shadows or situations heavily influenced by edge effects. As stated earlier in Chapter III the Shadow AOD program was run both with the minimum value shadow pixels and was also run with a modification using the pixel mean value. After running the program both ways, it was decided that the calculations using the mean values were more accurate for use as the primary data set as discussed below.

The first set of overall data to be shown will be from the data set using the minimum pixel value within the shaded region. Table 4 shows the overall AOD values

while Figures 13, 14, and 15 show the results broken down by the complete ROI set, the long shadow ROI set, and the short shadow ROI set respectively.

Table 4. Overall Shadow Method AOD results (minimum shaded pixel values). Mean Shadow Method AOD and standard deviation results for 76 ROIs taken from Beijing Sept 13, 2003. Calculations were made with minimum shaded pixel value.

Channel	Blue	Green	Red	NIR	Pan
Average	0.70	0.49	0.27	0.21	0.27
Standard Deviation	0.23	0.15	0.09	0.06	0.13

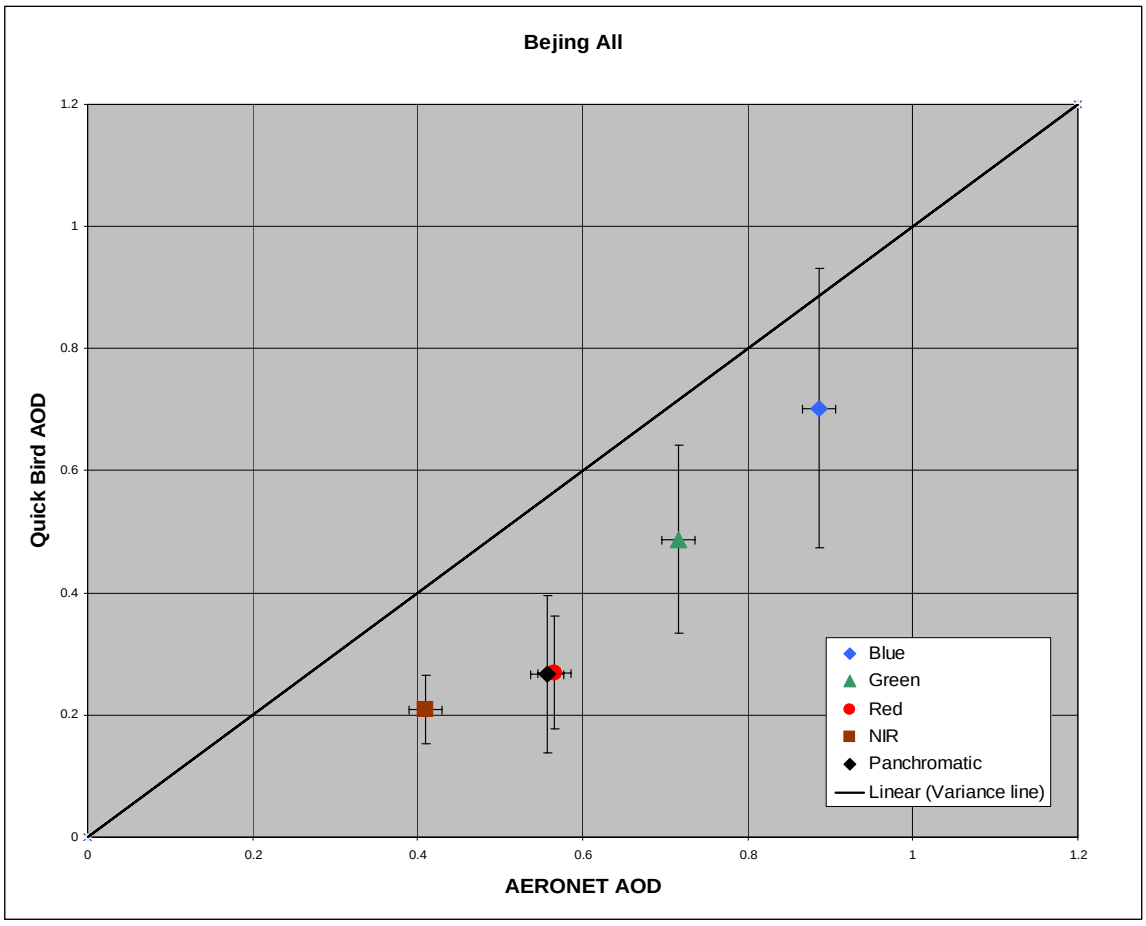

Figure 13. Comparison of QuickBird Shadow Method derived AOD with AERONET derived AOD for all ROIs of all surface types using minimum shaded pixel value for calculations. The vertical error bars indicated Shadow Method AOD standard deviation while the horizontal error bars indicate the uncertainty of the AERONET.

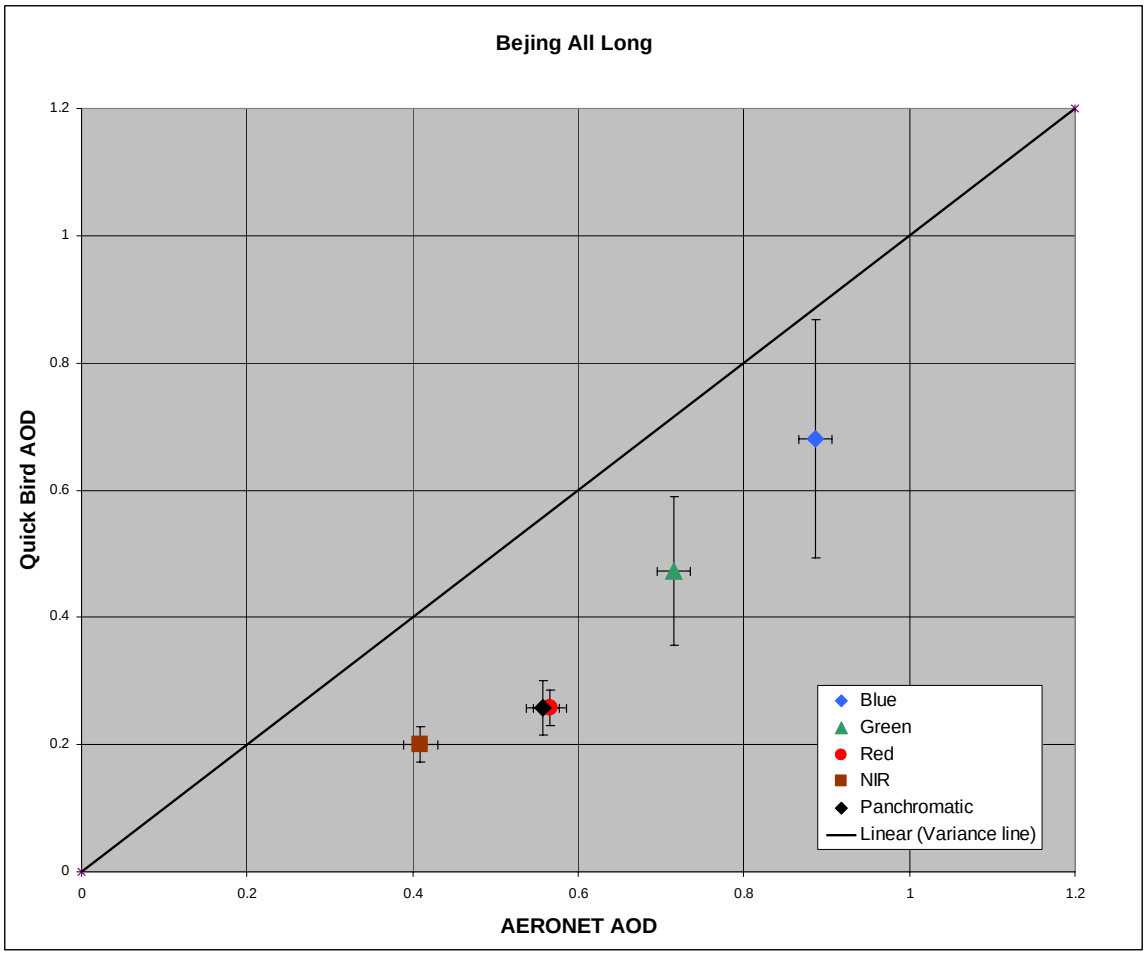

Figure 14. Comparison of QuickBird Shadow Method derived AOD with AERONET derived AOD for all ROIs with long shadows of all surface types using minimum shaded pixel value for calculations. The vertical error bars indicated Shadow Method AOD standard deviation while the horizontal error bars indicate the uncertainty of the AERONET.

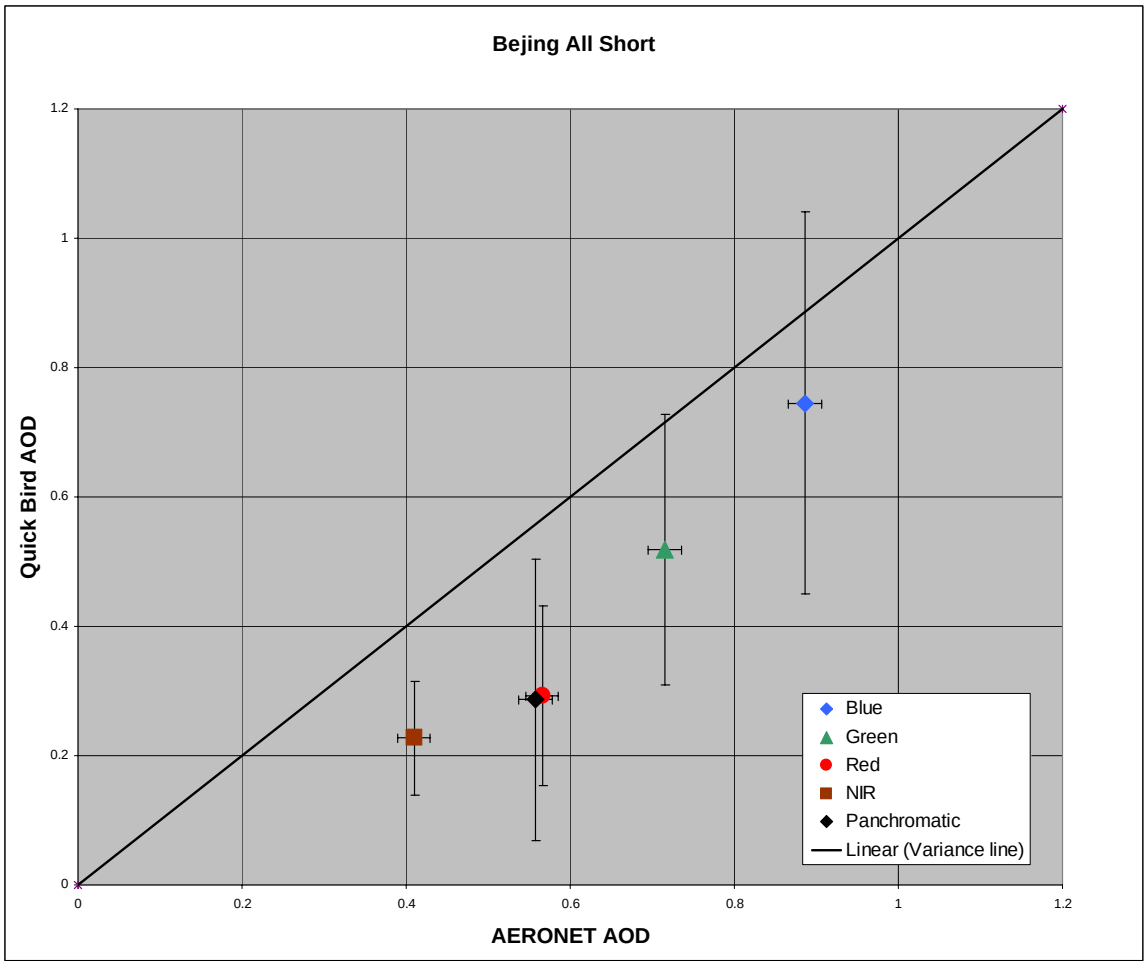

Figure 15. Comparison of QuickBird Shadow Method derived AOD with AERONET derived AOD for all ROIs with short shadows of all surface types using minimum shaded pixel value for calculations. The vertical error bars indicated Shadow Method AOD standard deviation while the horizontal error bars indicate the uncertainty of the AERONET.

The second set of overall data to be shown is from the data set using the mean pixel value within the shaded region. Table 5 shows the overall AOD values while Figures 16, 17, and 18 show the results broken down by the complete ROI set, the long shadow ROI set, and the short shadow ROI set respectively.

Table 5. Overall Shadow Method AOD results (mean shaded pixel values). Mean Shadow Method AOD and standard deviation results for 76 ROIs taken from Beijing Sept 13, 2003. Calculations were made with the mean shaded pixel value.

Channel	Blue	Green	Red	NIR	Pan
Average	0.79	0.52	0.29	0.22	0.30
Standard Deviation	0.32	0.14	0.09	0.04	0.05

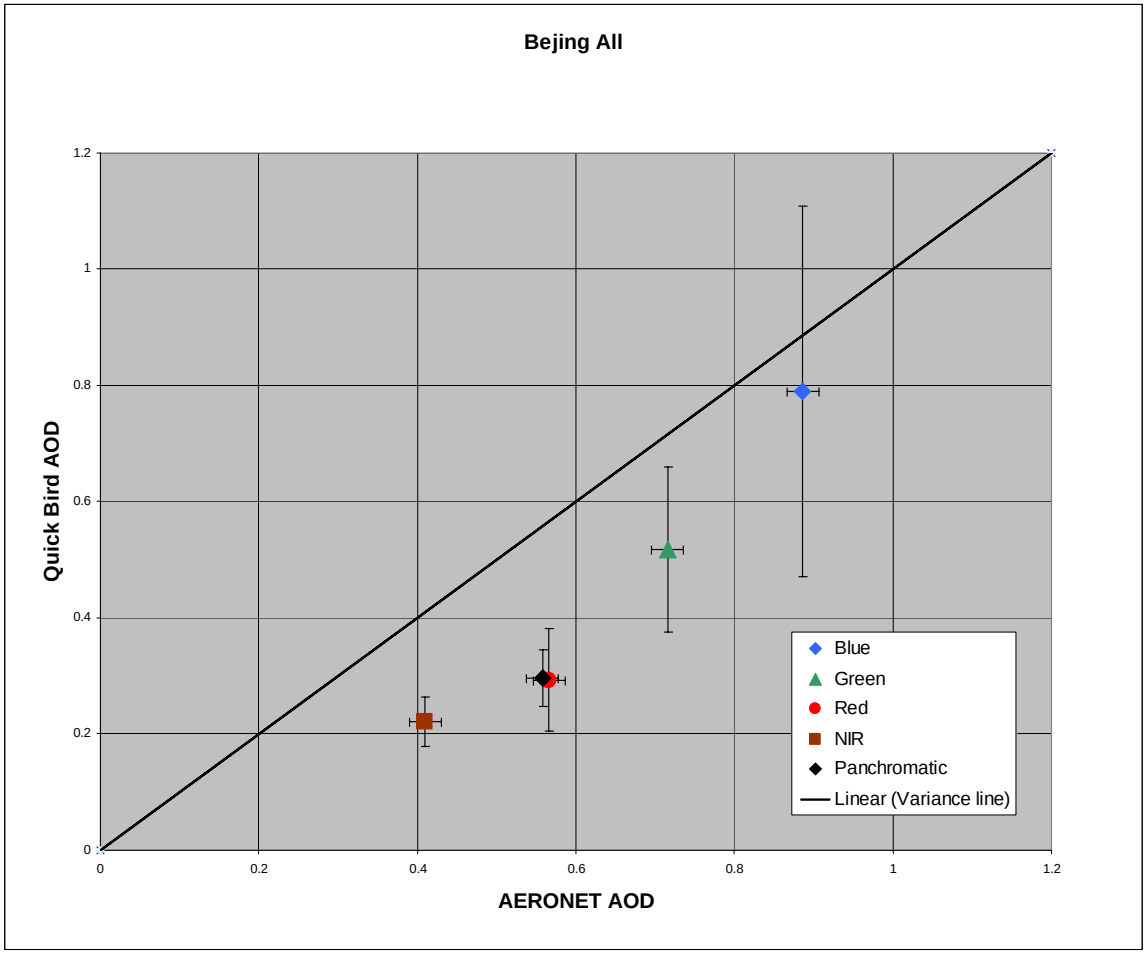

Figure 16. Comparison of QuickBird Shadow Method derived AOD with AERONET derived AOD for all ROIs of all surface types using the mean shaded pixel value for calculations. The vertical error bars indicated Shadow Method AOD standard deviation while the horizontal error bars indicate the uncertainty of the AERONET.

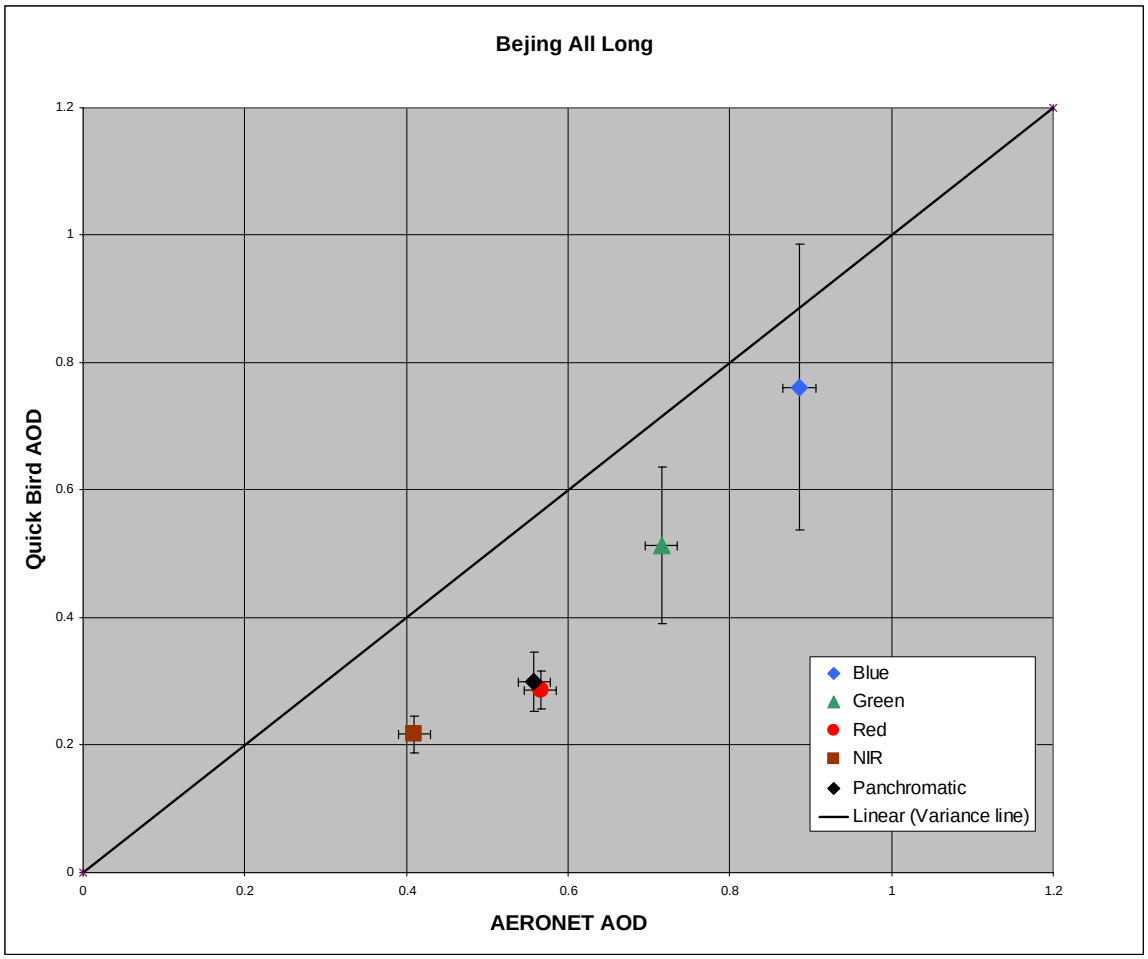

Figure 17. Comparison of QuickBird Shadow Method derived AOD with AERONET derived AOD for all ROIs with long shadows of all surface types using the mean shaded pixel value for calculations. The vertical error bars indicated Shadow Method AOD standard deviation while the horizontal error bars indicate the uncertainty of the AERONET.

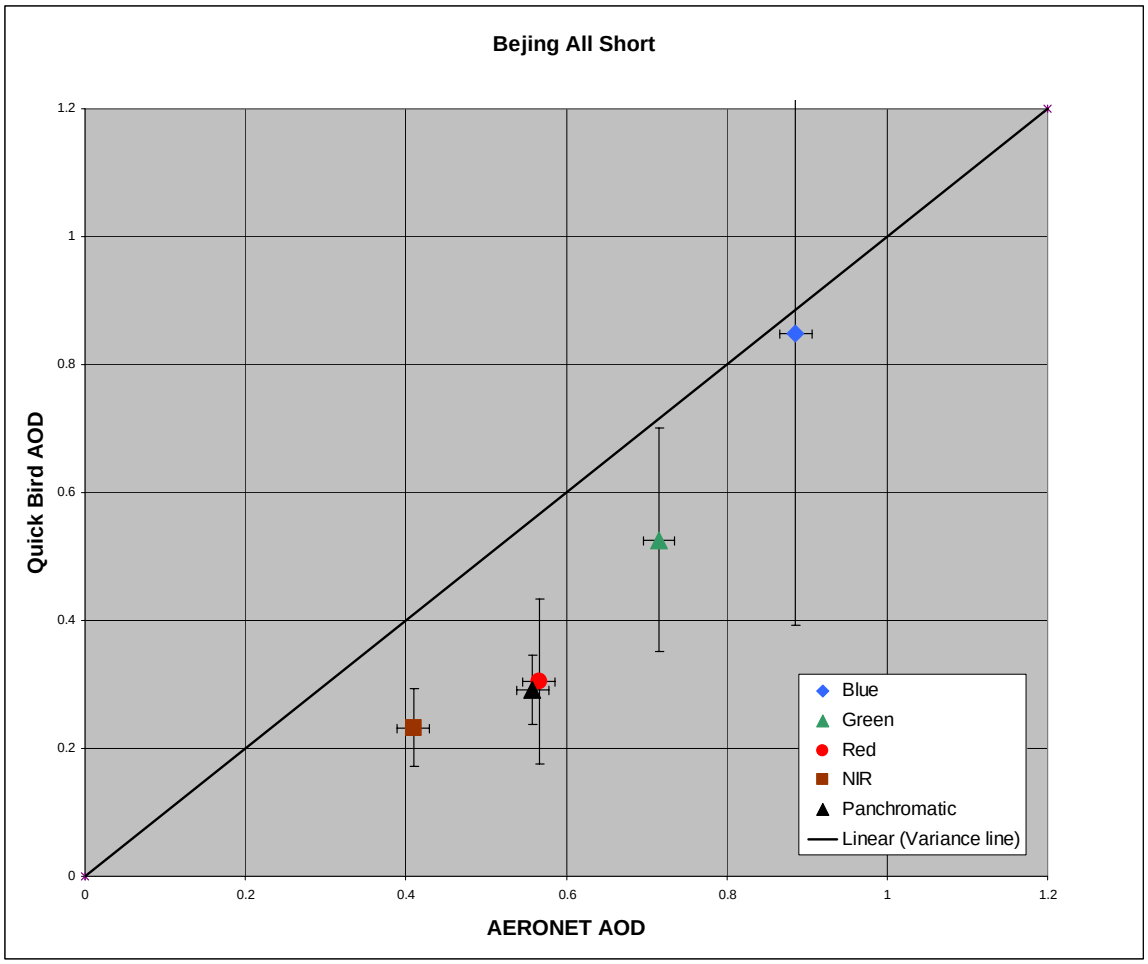

Figure 18. Comparison of QuickBird Shadow Method derived AOD with AERONET derived AOD for all ROIs with short shadows of all surface types using the mean shaded pixel value for calculations. The vertical error bars indicated Shadow Method AOD standard deviation while the horizontal error bars indicate the uncertainty of the AERONET.

Finally Table 6 does a direct comparison between the short and long shadow ROIs while Figure 19 graphically displays these results of the comparisons for all 76 ROIs across all five channels.

Table 6. Min vs. Mean AOD Comparison. AOD calculated using the mean radiance value with in the shaded region consistently gives a higher result than calculations made using the minimum pixel value depending on the respective channel.

All	Blue	Green	Red	NIR	Pan
Avg (mean) All ROIs	0.79	0.52	0.29	0.22	0.30
Avg (min) All ROIs	0.70	0.49	0.27	0.21	0.27
difference (mean-min)	0.09	0.03	0.02	0.01	0.03

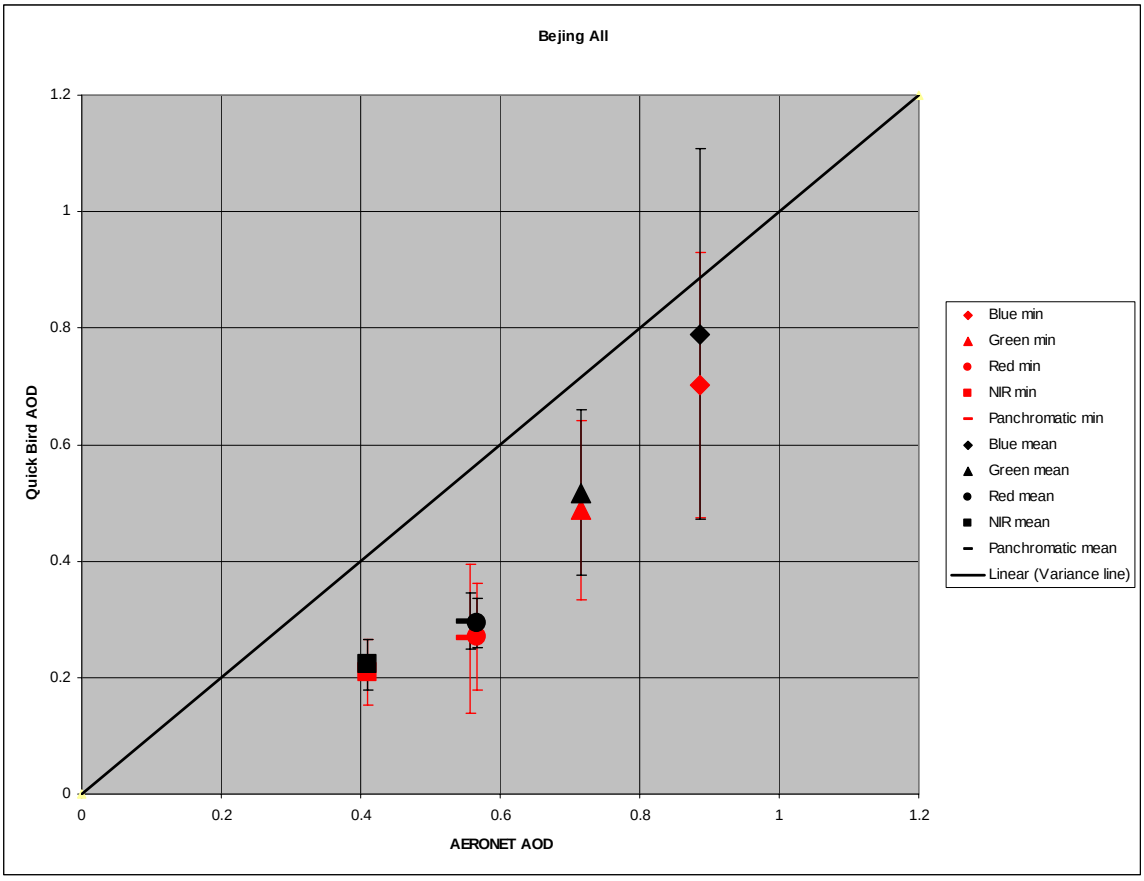

Figure 19. This figure graphically demonstrates the difference between the Shadow Method run with the minimum pixel radiance (in red) vs. the Shadow Method run using the mean pixel radiance (in black). The standard deviations are represented by the error bars.

When making the choice between which shadow values to use consideration for both the potential benefits and potential errors that each can introduce should be accounted for. One possible error that can be introduced by using the minimum pixel value is contamination of the homogeneous background by sub-pixel objects. In the ROI

selection process it was noted several times, especially with grass backgrounds, that there were dark bushes in the scenes that did not show up in the multi-spectral (relatively low resolution) shots, but did show up in the higher panchromatic resolution scenes. The lack of being able to distinguish these features can lead to a pixel in the shadow region that registers darker than the background really is and is even affected to a greater extent if only the darkest pixel is used. Therefore, when using a darkest pixel method chances of contamination are increased. If this happens, the shadow effectively registers as darker than reality, which increases the difference between the shaded and non-shaded region and decreases the calculated AOD value. This would generally increase the standard deviation.

In every case, as seen in Figure 19, calculations made using the mean radiance value vs. the minimum radiance value do result in an increase in the calculated AOD. This increase moves the calculated results closer to the true answer. This does not explicitly show that using the mean value is better. There is an obvious low bias to all the calculations even with the increase associated with the use of the mean radiance values inside the shadow. Until we can account for this bias we can not specifically say which AOD calculation is better.

Another observation that stands out is the change in the standard deviation between the two runs. In every case except the blue channel, the standard deviation decreases with the use of mean values indicating an increase of consistency. Not only does the blue channel's standard deviation not decrease, it actually increases at a rate higher than all the other channels decrease. The reason for this deviation from the decrease in the standard deviation is not clear. Because of the reasons stated above, the results below use the mean pixel value within the shaded region to perform the Shadow Method AOD calculations

C. OVERALL RESULTS

This section will look at the overall results of the Shadow Method as it is broken down by both the surface type and shadow length. The results from all ROIs, for the long

and short shadow cases for all surface types are listed in Tables 7-9 and displayed in Figures 20-22 respectively.

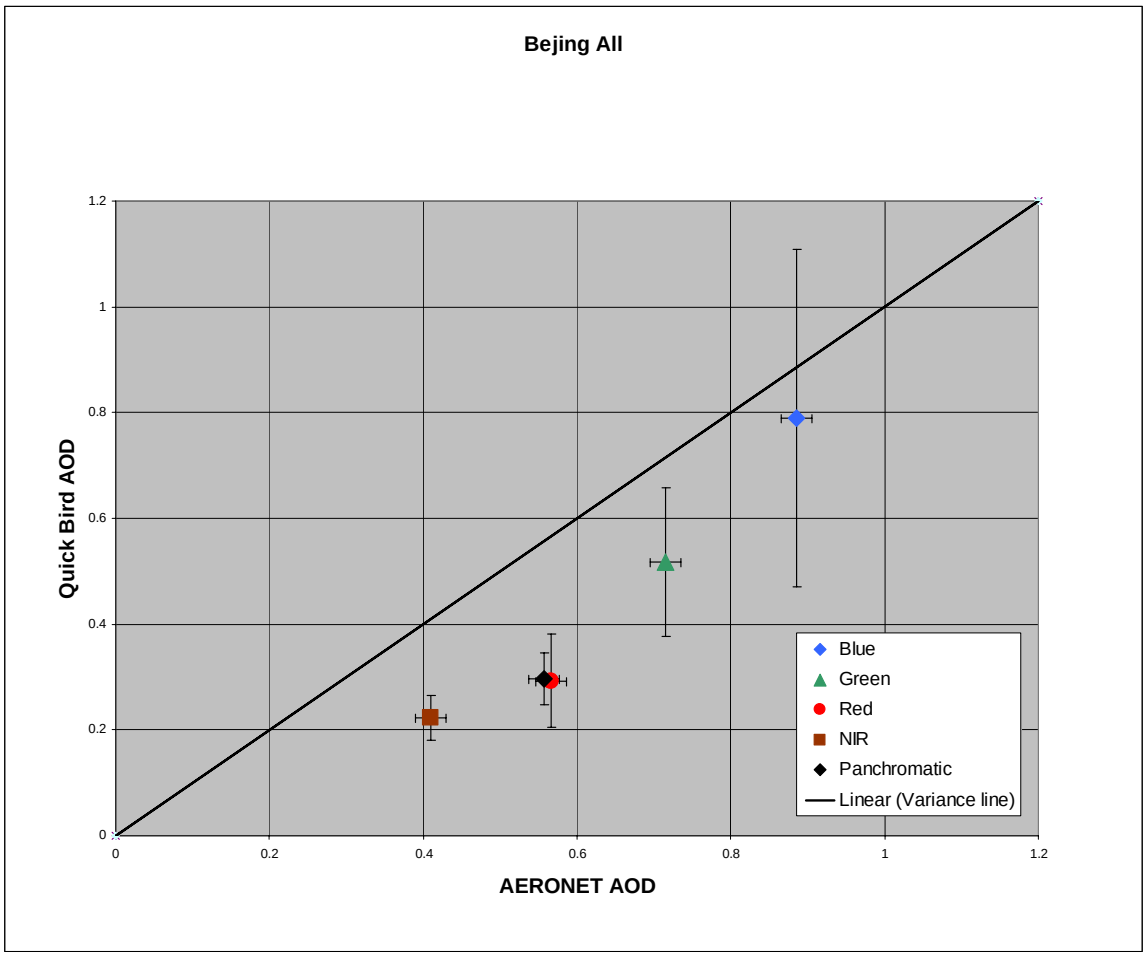

Figure 20. Comparison of QuickBird Shadow Method derived AOD with AERONET derived AOD for ROIs of all surface types and all shadow lengths. The vertical error bars indicated Shadow Method AOD standard deviation while the horizontal error bars indicate the uncertainty of the AERONET.

Table 7. Overall Shadow Method AOD all surface types. Shadow Method AOD results for ROIs of all surface types and all shadow lengths.

Channel	Blue	Green	Red	NIR	Pan
Mean (all)	0.79	0.52	0.29	0.22	0.30
Standard Deviation	0.32	0.14	0.09	0.04	0.05

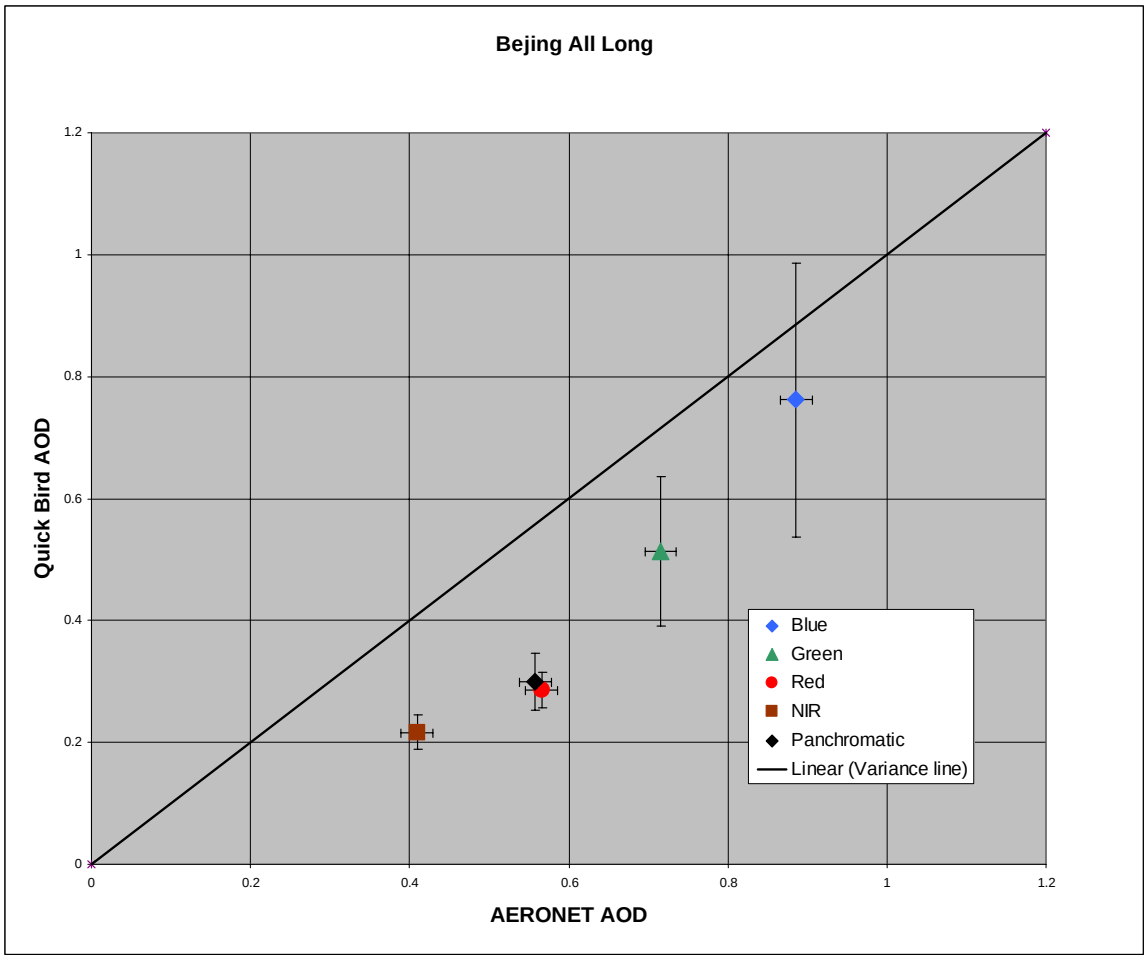

Figure 21. Comparison of QuickBird Shadow Method derived AOD with AERONET derived AOD for ROIs of all surface types and long shadows. The vertical error bars indicated Shadow Method AOD standard deviation while the horizontal error bars indicate the uncertainty of the AERONET.

Table 8. Overall Shadow Method AOD all surface types and long shadows. Shadow Method AOD results for ROIs of all surface types and all shadow lengths.

Channel	Blue	Green	Red	NIR	Pan
Mean (long)	0.76	0.51	0.29	0.22	0.30
Standard Deviation	0.22	0.12	0.06	0.03	0.05

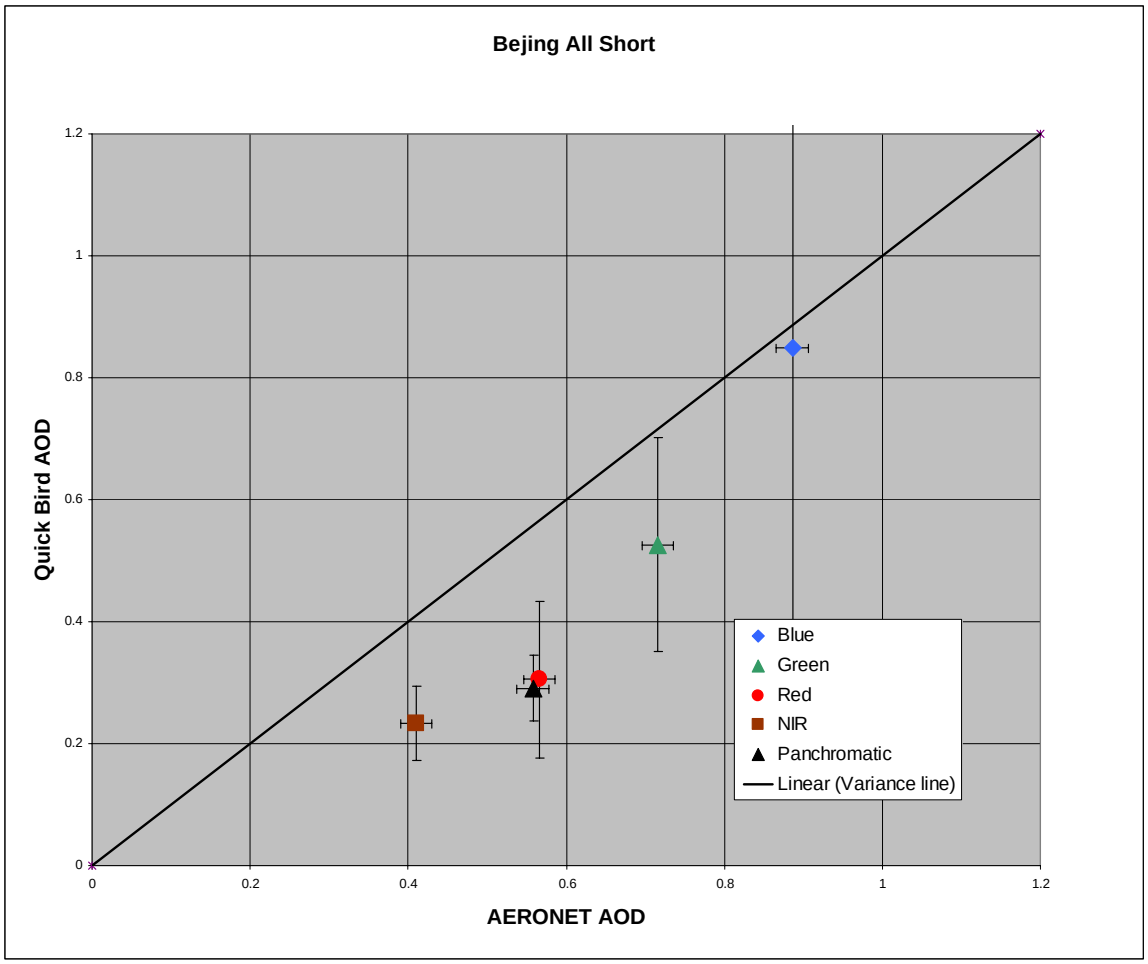

Figure 22. Comparison of QuickBird Shadow Method derived AOD with AERONET derived AOD for ROIs of all surface types and short shadows. The vertical error bars indicated Shadow Method AOD standard deviation while the horizontal error bars indicate the uncertainty of the AERONET.

Table 9. Overall Shadow Method AOD all surface types and short shadows. Shadow Method AOD results for ROIs of all surface types and all shadow lengths.

Channel	Blue	Green	Red	NIR	Pan
Mean (short)	0.85	0.53	0.31	0.23	0.29
Standard Deviation	0.46	0.18	0.13	0.06	0.05

After viewing the results from the entire scene there are two observations that stand out. The first is that there is an overall low bias across all the QuickBird channels. This bias is fairly uniform and seen in both the long and short shadow cases. The

apparent cause of this bias has not yet been determined. The second observation is that the standard deviations have an inverse relationship with wavelength. In other words the standard deviation decreases as the wavelength increase. This is believed to be due to the decrease of the affect that Rayleigh scattering has as wavelength is increased.

Table 10. AERONET vs. mean Shadow Method AOD comparison. This table quantifies the average bias or error in the shadow method relative to the AERONET for all ROIs. Note the strong low bias in the results.

Channel	Blue	Green	Red	NIR	Pan
Shadow Method derive AOD	0.79	0.52	0.29	0.22	0.30
AERONET AOD	0.89	0.72	0.57	0.41	0.56
Change/Bias	-0.10	-0.20	-0.27	-0.19	-0.26

As discussed earlier, edge effects are one of the main forms of contamination to be concerned with. In order to explore the potential edge effect problem the shadows were categorized as being short shadows and long shadows. Assuming Lambertian reflectance, short shadows are believed to act to drive up the calculated AOD. In situations with short shadows, four pixels or less, the outside pixels are most likely to be partially filled by either non-shaded surface from outside the shaded region or by the shadow caster on the other side. This partial pixel filling acts to increase the radiance value inside these particular pixels. The shadows therefore register as being brighter. The brighter shadows decrease the shaded to non-shaded difference which in turn increases the calculated AOD. In most cases based on the orientation of the shadow relative to the directions of the pixels, it can be quite difficult to determine exactly where edge effects begin or end.

When viewing the data for the means of all the short shadow ROIs and the means for all the long shadow ROIs this theory seems to hold true. This can be seen in Table 11. The effect is not strong in the green, red, and NIR channels. The effect is strong in the blue channel is most likely due to the particularly strong signal seen in the blue channel over grass surfaces. This, however, does not necessarily hold true when looking at specific surface results.

Table 11. Long vs. Short AOD analysis, all ROIs. Analysis of the mean values for all ROIs indicate that the Shadow Method calculations for short shadows tend to produce higher AODs overall.

Channel	Blue	Green	Red	NIR
Long shadows	0.76	0.51	0.29	0.22
Short shadows	0.85	0.53	0.31	0.23
Difference short-long	0.09	0.01	0.02	0.02

D. SURFACE SPECIFIC RESULTS

This section will describe the results of the Shadow Method as it is broken down by both the surface type and shadow length.

1. ROIs, Dirt Surfaces

The results for all of the dirt ROIs, the long shadow dirt cases, and short shadow dirt cases, are listed in Tables 23-25 and displayed in Figures 19-21 respectively.

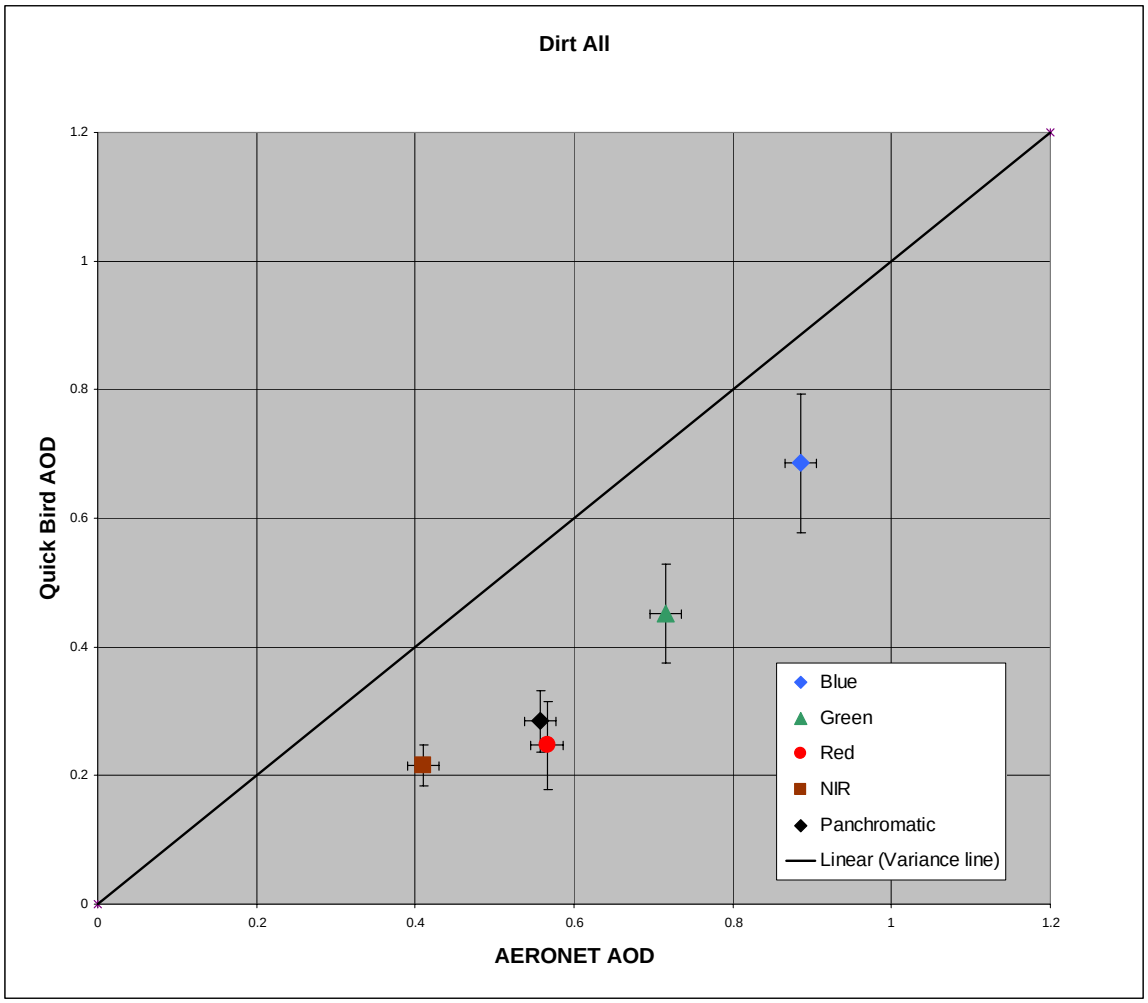

Figure 23. Comparison of QuickBird Shadow Method derived AOD with AERONET derived AOD for ROIs of all dirt surfaces and all shadow lengths. The vertical error bars indicated Shadow Method AOD standard deviation while the horizontal error bars indicate the uncertainty of the AERONET.

Table 12. Shadow Method AOD dirt surface. Shadow Method AOD results for ROIs of dirt surfaces and all shadow lengths.

Channel	Blue	Green	Red	NIR	Pan
Mean (all)	0.69	0.45	0.25	0.22	0.28
Standard Deviation	0.11	0.08	0.07	0.03	0.05

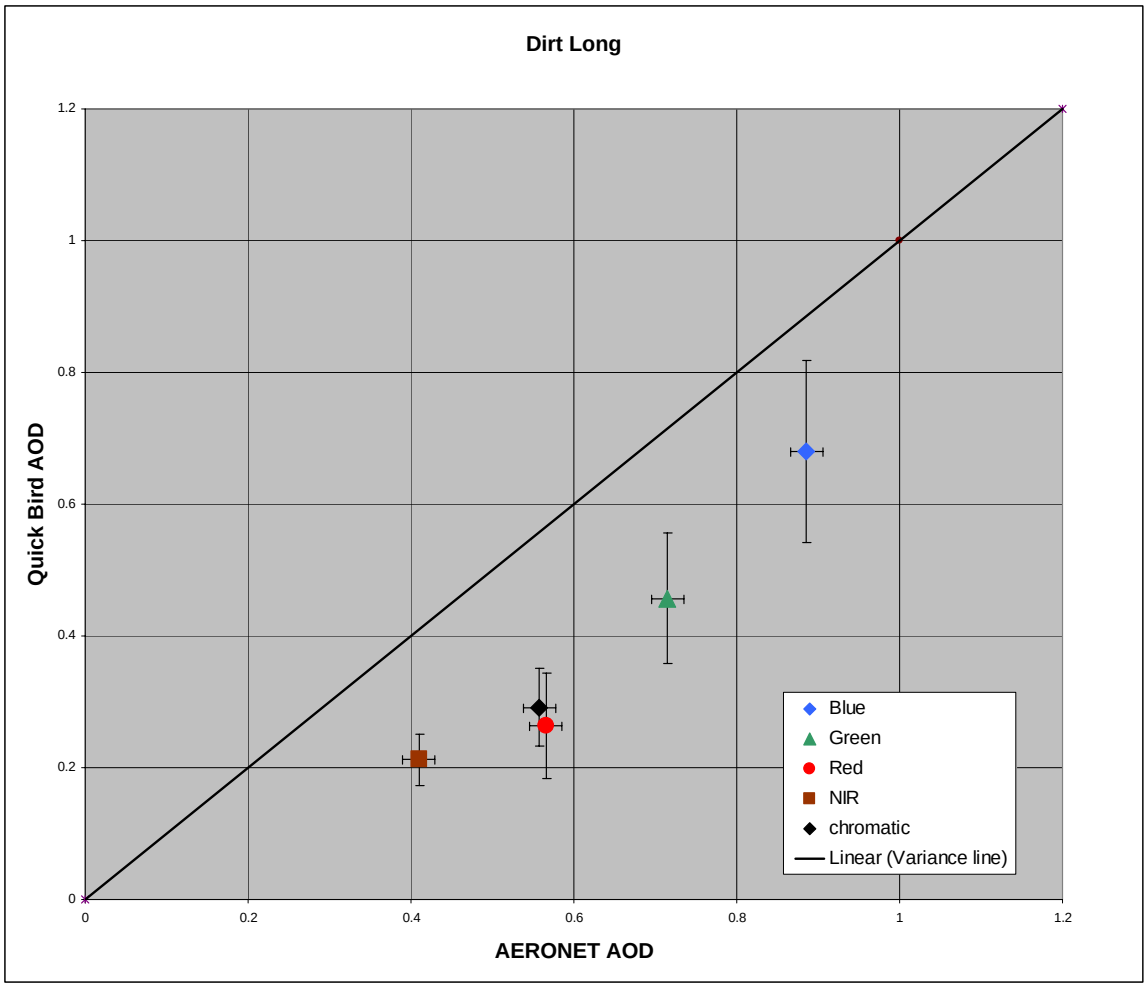

Figure 24. Comparison of QuickBird Shadow Method derived AOD with AERONET derived AOD for ROIs of all dirt surfaces with long shadows. The vertical error bars indicated Shadow Method AOD standard deviation while the horizontal error bars indicate the uncertainty of the AERONET.

Table 13. Shadow Method AOD dirt surface long shadows. Shadow Method AOD results for ROIs of dirt surfaces and long shadows.

Channel	Blue	Green	Red	NIR	Pan
Mean (long)	0.68	0.46	0.26	0.21	0.29
Standard Deviation	0.14	0.10	0.08	0.04	0.06

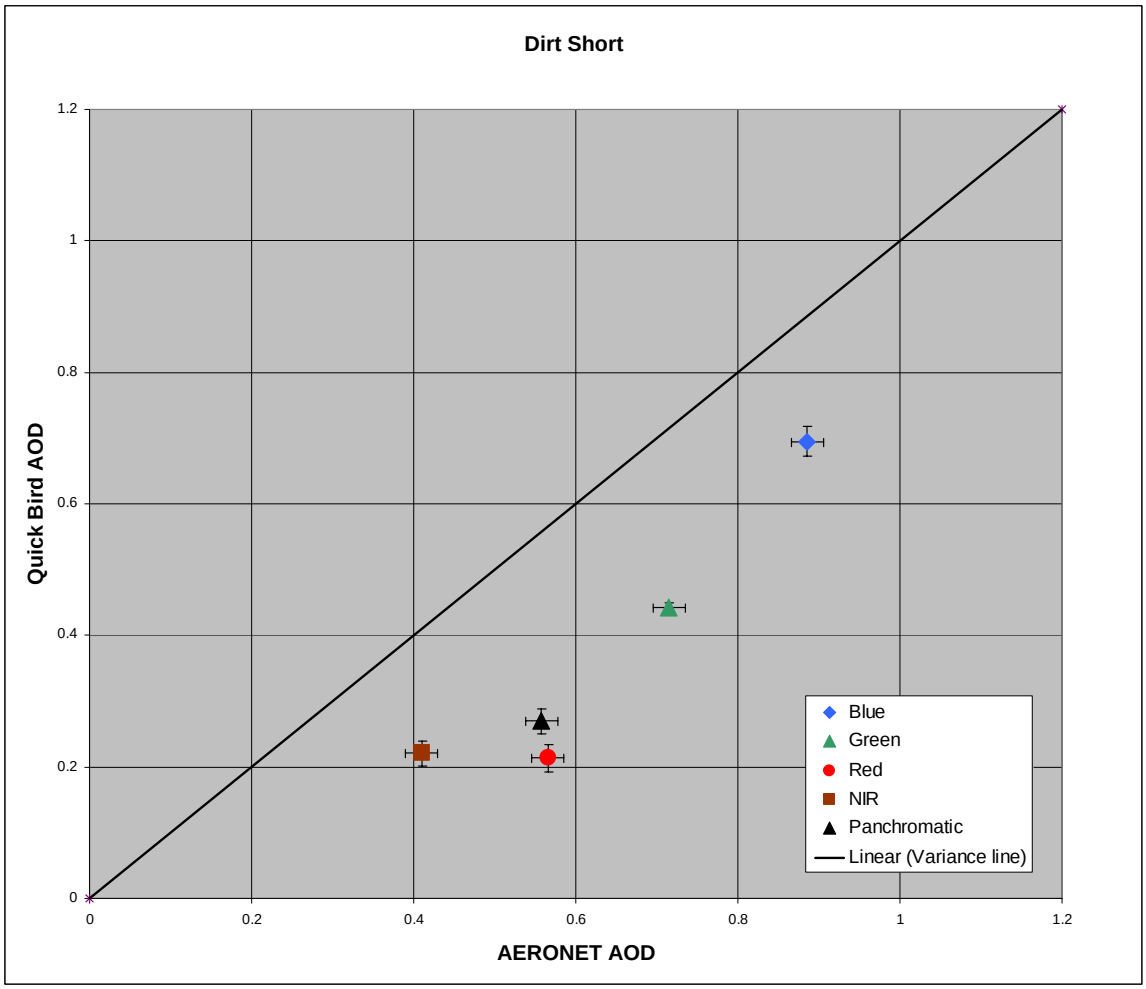

Figure 25. Comparison of QuickBird Shadow Method derived AOD with AERONET derived AOD for ROIs of dirt surface with short shadows. The vertical error bars indicated Shadow Method AOD standard deviation while the horizontal error bars indicate the uncertainty of the AERONET.

Table 14. Shadow Method AOD dirt surface with short shadows. Shadow Method AOD results for ROIs of dirt surfaces and short shadows.

Channel	Blue	Green	Red	NIR	Pan
Mean (short)	0.70	0.44	0.21	0.22	0.27
Standard Deviation	0.02	0.01	0.02	0.02	0.02

After reviewing the results from the dirt ROI cases, it is evident that the dirt ROIs demonstrate the same characteristics that the overall results demonstrate. The one difference is that there is an extremely low standard deviation relative to the overall results and other surface types. This is believed to be attributed to the relative small

sample size of only six ROIs. Though the sample size is small and more cases should be used to confirm the results, the results should not be discounted considering the extent that they match the rest of the results.

When comparing the results between the long and short shadows the calculations provide mixed results compared to the expected outcome. The AOD differences are weak in all the channels except the red channel where the long shadow results provide a higher AOD than the short shadow. It must be noted that the fairly small sample set can skew these results also. The results can be seen in Table 15.

Table 15. Long vs. Short AOD analysis, Dirt ROIs. Analysis of the mean values for all dirt ROIs indicate that the Shadow Method provides mixed results with respect to long vs. short shadows among the separate channels. It must be noted that results are questionable with dirt ROIs due to a relatively small sample size.

Channel	Blue	Green	Red	NIR
Long shadows	0.68	0.46	0.26	0.21
Short shadows	0.70	0.44	0.21	0.22
Difference short-long	0.01	-0.01	-0.05	0.01

2. ROIs, Grass Surfaces

The mean AOD for all grass ROIs, long shadow grass cases, and short shadow grass cases, are listed in Tables 16-18 and displayed in Figures 26-28 respectively.

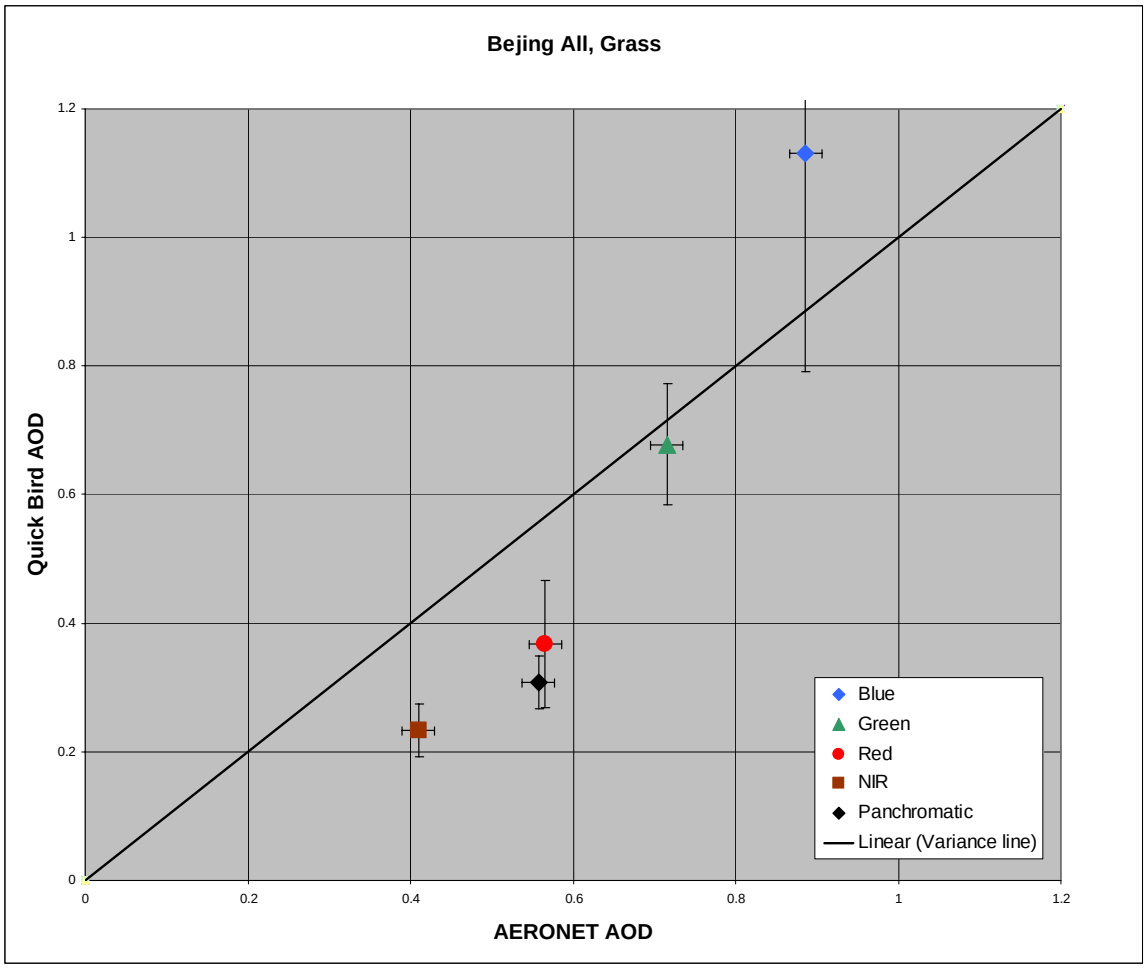

Figure 26. Comparison of QuickBird Shadow Method derived AOD with AERONET derived AOD for ROIs of all grass surfaces and all shadow lengths. The vertical error bars indicated Shadow Method AOD standard deviation while the horizontal error bars indicate the uncertainty of the AERONET.

Table 16. Shadow Method AOD grass surface. Shadow Method AOD results for ROIs of grass surfaces and all shadow lengths.

Channel	Blue	Green	Red	NIR	Pan
Mean (all)	1.13	0.68	0.37	0.23	0.31
Standard Deviation	0.34	0.09	0.10	0.04	0.04

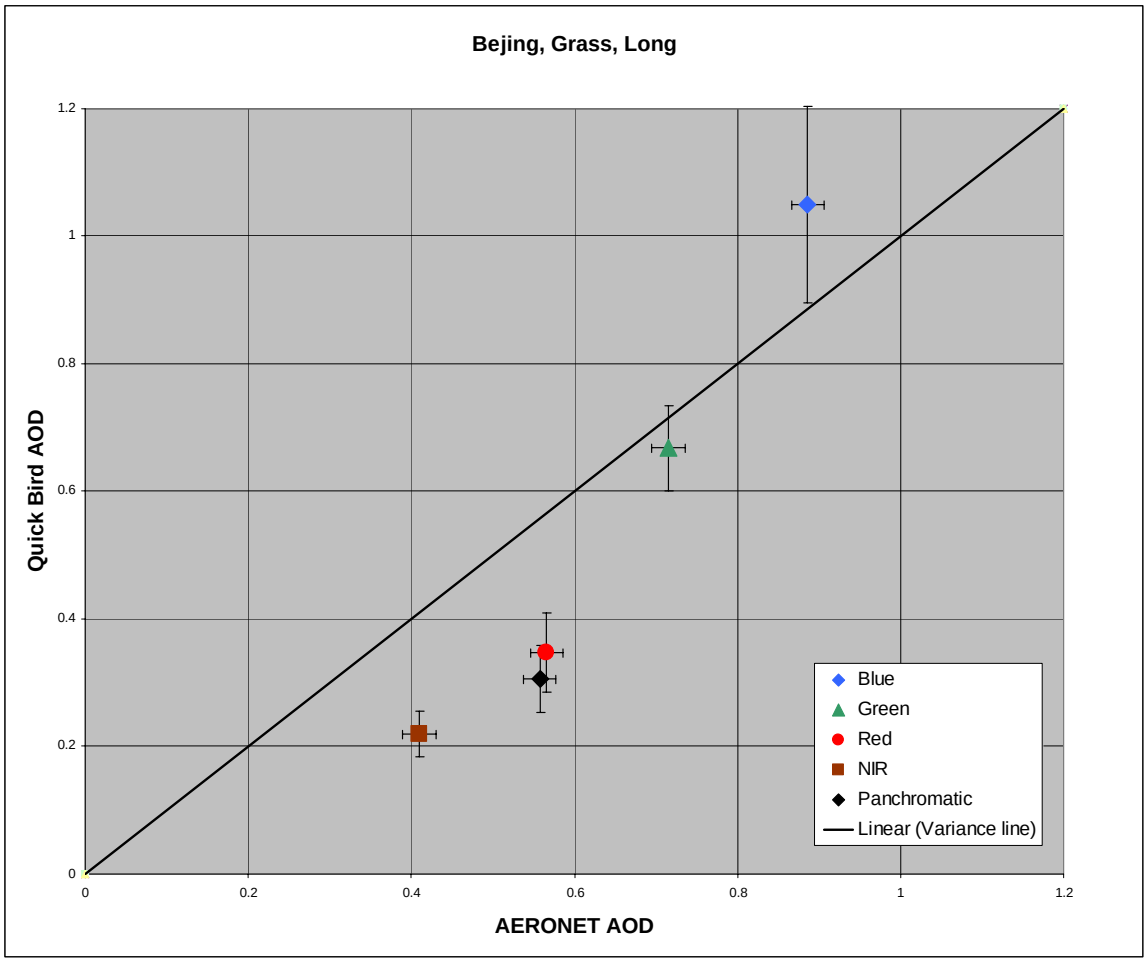

Figure 27. Comparison of QuickBird Shadow Method derived AOD with AERONET derived AOD for ROIs of all grass surfaces with long shadows. The vertical error bars indicated Shadow Method AOD standard deviation while the horizontal error bars indicate the uncertainty of the AERONET.

Table 17. Shadow Method AOD grass surface long shadows. Shadow Method AOD results for ROIs of grass surfaces and long shadows.

Channel	Blue	Green	Red	NIR	Pan
Mean (long)	1.05	0.67	0.35	0.22	0.31
Standard Deviation	0.15	0.07	0.06	0.04	0.05

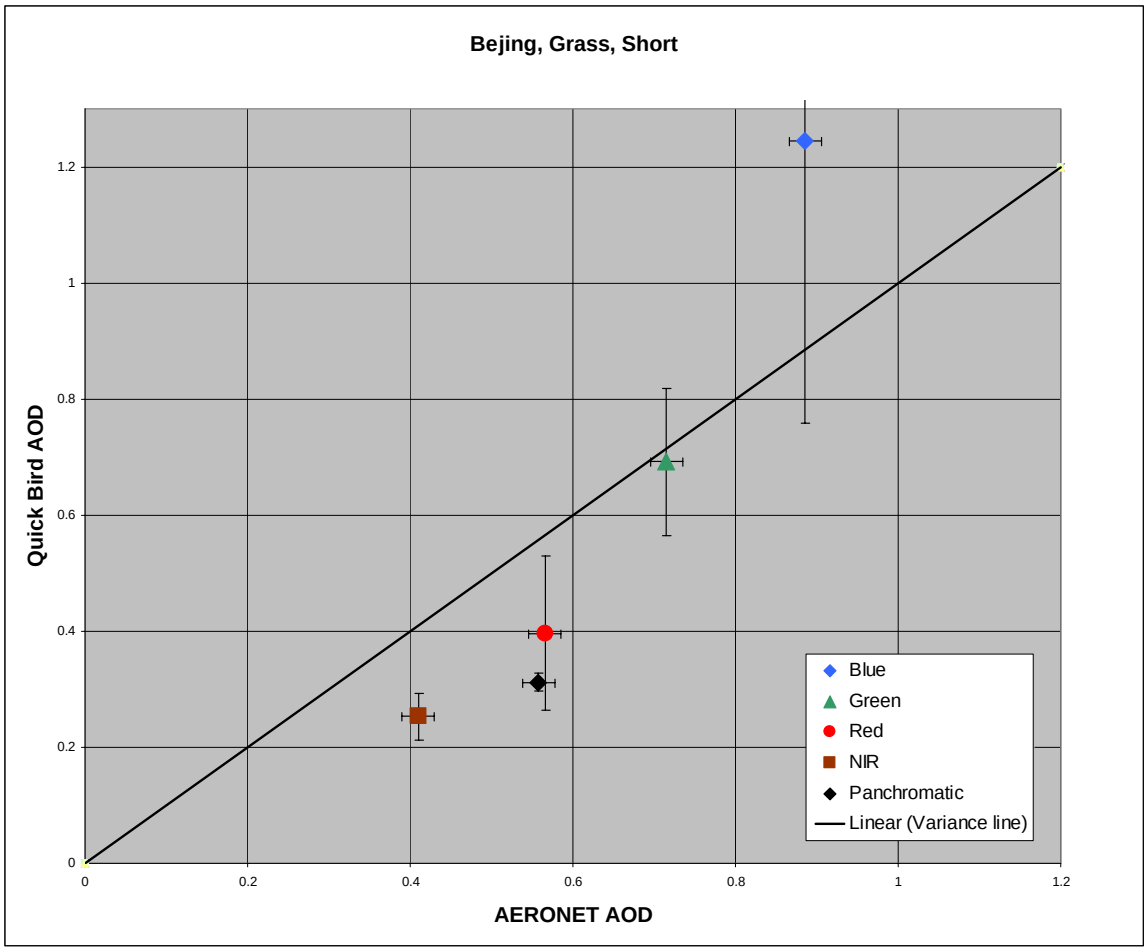

Figure 28. Comparison of QuickBird Shadow Method derived AOD with AERONET derived AOD for ROIs of grass surfaces with short shadows. The vertical error bars indicated Shadow Method AOD standard deviation while the horizontal error bars indicate the uncertainty of the AERONET.

Table 18. Shadow Method AOD grass surface with short shadows. Shadow Method AOD results for ROIs of grass surfaces and short shadows.

Channel	Blue	Green	Red	NIR	Pan
Mean (short)	1.24	0.69	0.40	0.25	0.31
Standard Deviation	0.49	0.13	0.13	0.04	0.02

After reviewing the results from the grass ROI cases, it is evident that the grass ROIs deviate from the general pattern of low bias that is observed in all the other surface types. The blue and green channels show a significantly higher AOD than is observed with other surfaces. The reason for this deviation is not completely apparent. Out of all

the surface types grass is the least reflective particularly in the shorter wavelengths. The Shadow Method relies on high reflectance for accurate results. It is hypothesized that the surface reflactance estimations performed by the Shadow Method IDL program may have difficulty when dealing with weakly reflective surfaces. To compound the problem the atmosphere is quite optically thick in the shorter wave lengths due to Rayleigh scattering. This increase in optical thickness acts to decrease the difference between the shaded and unshaded regions of the ROI. Sensitivity tests performed by Vincent (2006) showed that accuracy begins to decrease when the shaded to non-shaded difference falls below 10 Wm^2. In the grass cases the difference was typically well below this threshold. This also can explain the larger standard deviations observed with this surface type.

When comparing the results between the long and short shadows the calculations provide expected results. The short shadows typically showed higher AODs than the long shadow cases. The results can be seen in Table 19.

Table 19. Long vs. Short AOD analysis, Grass ROIs. Analysis of the mean values for all grass ROIs indicate that the Shadow Method calculations for short shadows tend to produce higher AODs than long shadows.

Channel	Blue	Green	Red	NIR
Long shadows	1.05	0.67	0.35	0.22
Short shadows	1.24	0.69	0.40	0.25
Difference short-long	0.19	0.02	0.05	0.03

3. ROIs, Pavement Surfaces

The all pavement ROIs results for long pavement shadow cases and short pavement shadow cases, are listed in Tables 29-31 and displayed in Figures 25-27 respectively.

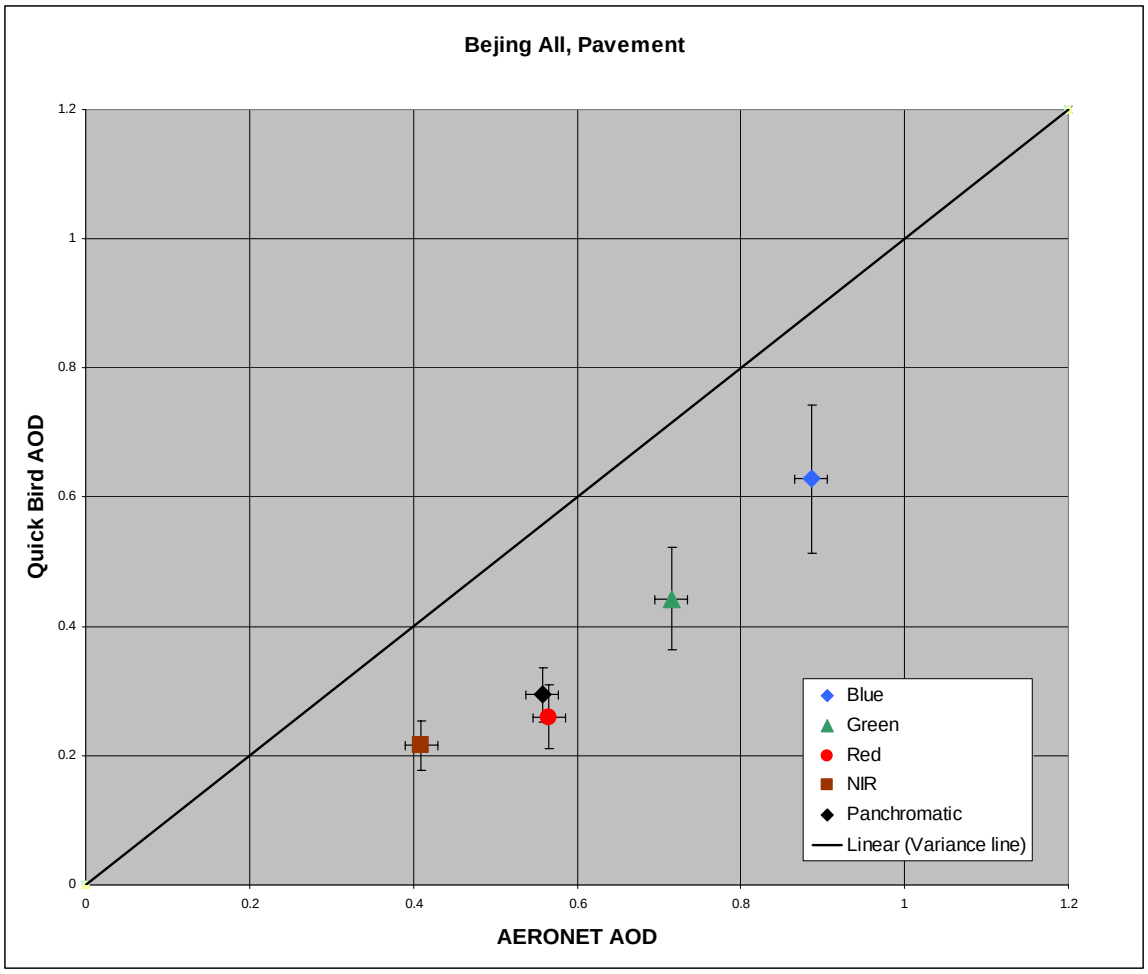

Figure 29. Comparison of QuickBird Shadow Method derived AOD with AERONET derived AOD for ROIs of all pavement surfaces and all shadow lengths. The vertical error bars indicated Shadow Method AOD standard deviation while the horizontal error bars indicate the uncertainty of the AERONET.

Table 20. Shadow Method AOD pavement surface. Shadow Method AOD results for both short and long shadow ROIs for pavement surfaces.

Channel	Blue	Green	Red	NIR	Pan
Mean (all)	0.63	0.44	0.26	0.22	0.29
Standard Deviation	0.12	0.08	0.05	0.04	0.04

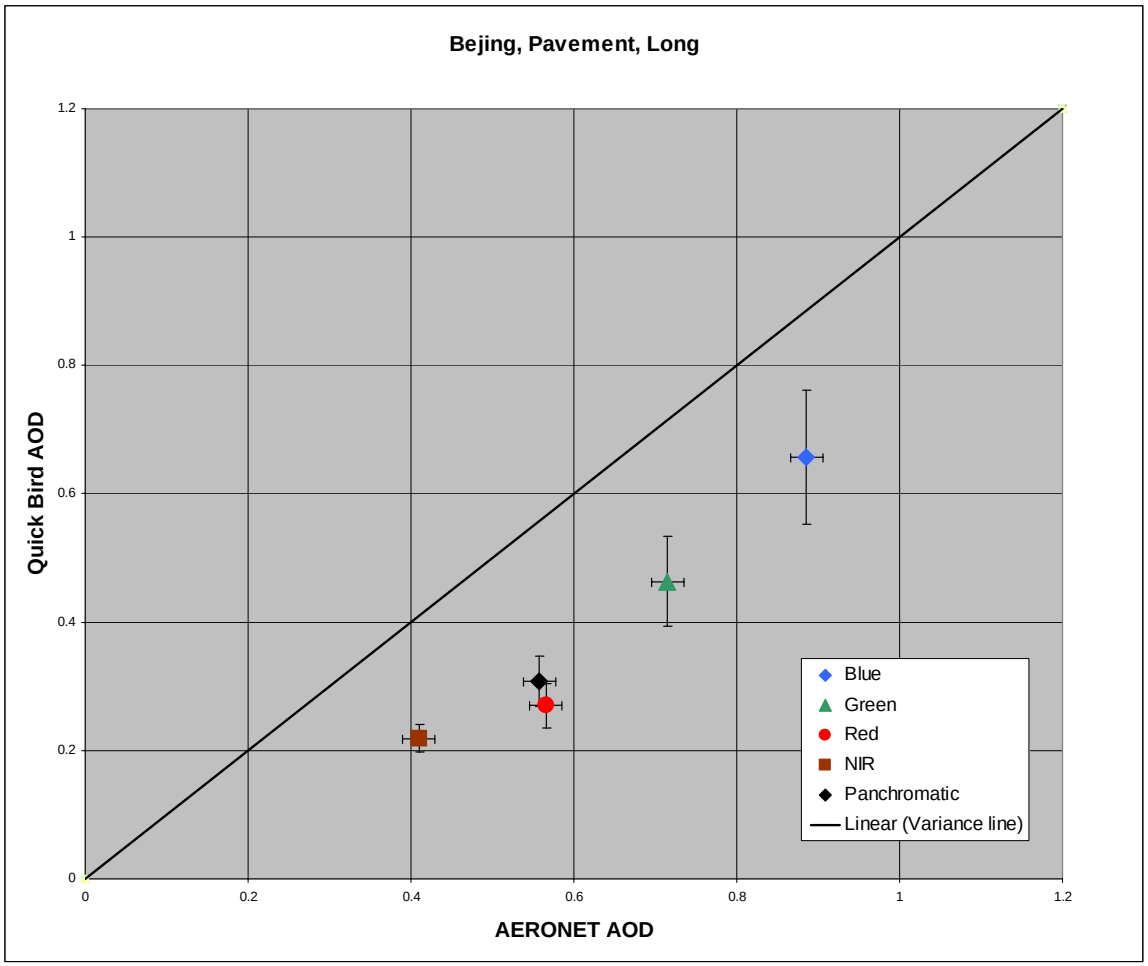

Figure 30. Comparison of QuickBird Shadow Method derived AOD with AERONET derived AOD for ROIs of all pavement surfaces with long shadows. The vertical error bars indicated Shadow Method AOD standard deviation while the horizontal error bars indicate the uncertainty of the AERONET.

Table 21. Shadow Method AOD pavement surface long shadows. Shadow Method AOD results for ROIs of pavement surfaces and long shadows.

Channel	Blue	Green	Red	NIR	Pan
Mean (long)	0.66	0.46	0.27	0.22	0.31
Standard Deviation	0.10	0.07	0.04	0.02	0.04

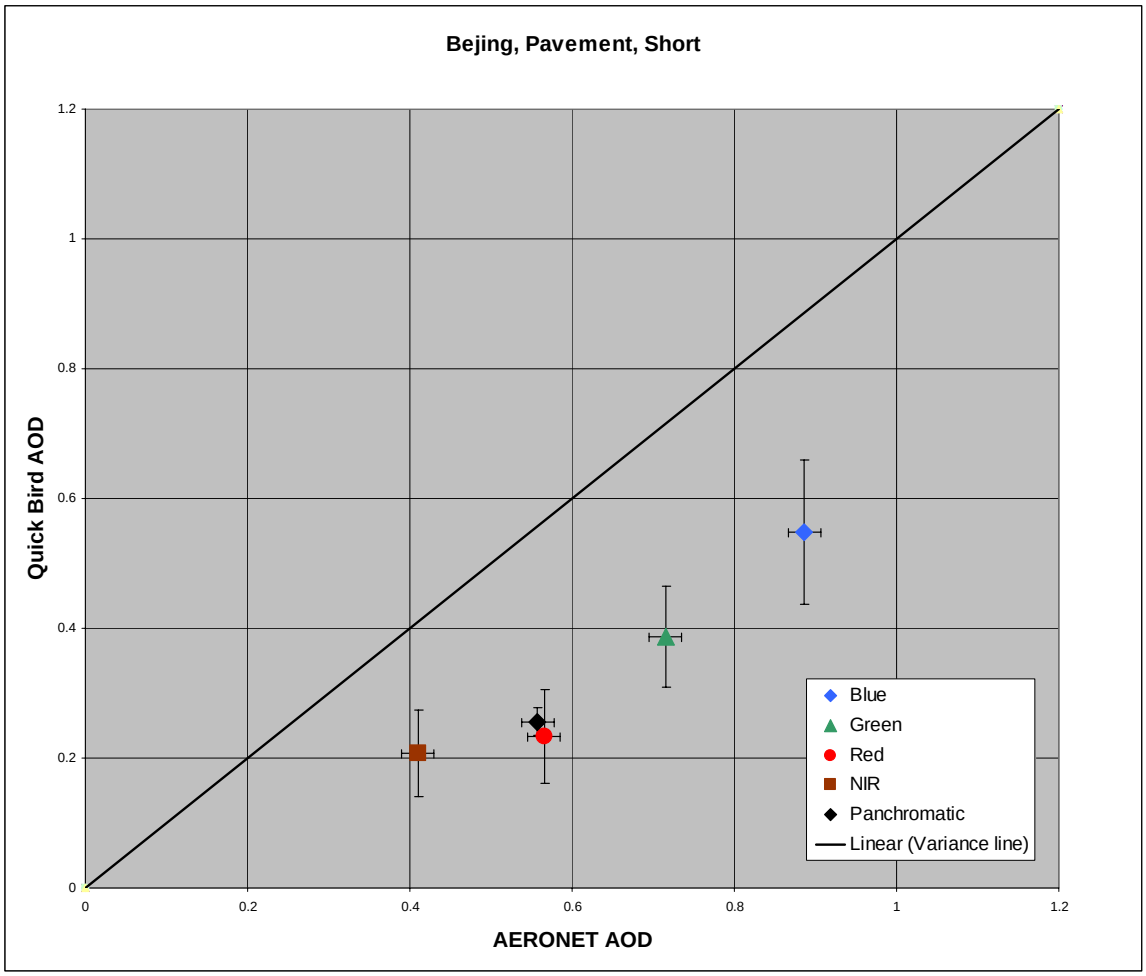

Figure 31. Comparison of QuickBird Shadow Method derived AOD with AERONET derived AOD for ROIs of pavement surfaces with short shadows. The vertical error bars indicated Shadow Method AOD standard deviation while the horizontal error bars indicate the uncertainty of the AERONET.

Table 22. Shadow Method AOD pavement surface with short shadows. Shadow Method AOD results for ROIs of pavement surfaces and short shadows.

Channel	Blue	Green	Red	NIR	Pan
Mean (short)	0.55	0.39	0.23	0.21	0.26
Standard Deviation	0.11	0.08	0.07	0.07	0.02

After reviewing the results from the pavement ROI cases, it is evident that the pavement ROIs have the same characteristics as the overall results.

When comparing the results between the long and short shadows the calculations provide opposite results from the higher AODs expected. The short shadows display lower AODs than observed in the long shadows. The cause for this deviation in not understood. The results are shown in Table 23.

Table 23. Long vs. short AOD analysis, Pavement ROIs. Analysis of the mean values for all pavement ROIs indicate that the Shadow Method calculations for short shadows tend to produce lower AODs than long shadows contradictory to the overall trend.

Channel	Blue	Green	Red	NIR
Long shadows	0.66	0.46	0.27	0.22
Short shadows	0.55	0.39	0.23	0.21
Difference short-long	-0.11	-0.08	-0.04	-0.01

4. ROIs, Other Surfaces

The all OTHER ROIs results, long “other” shadow cases, and short “other” shadow cases, are listed in Tables 32-34 and displayed in Figures 28-30 respectively.

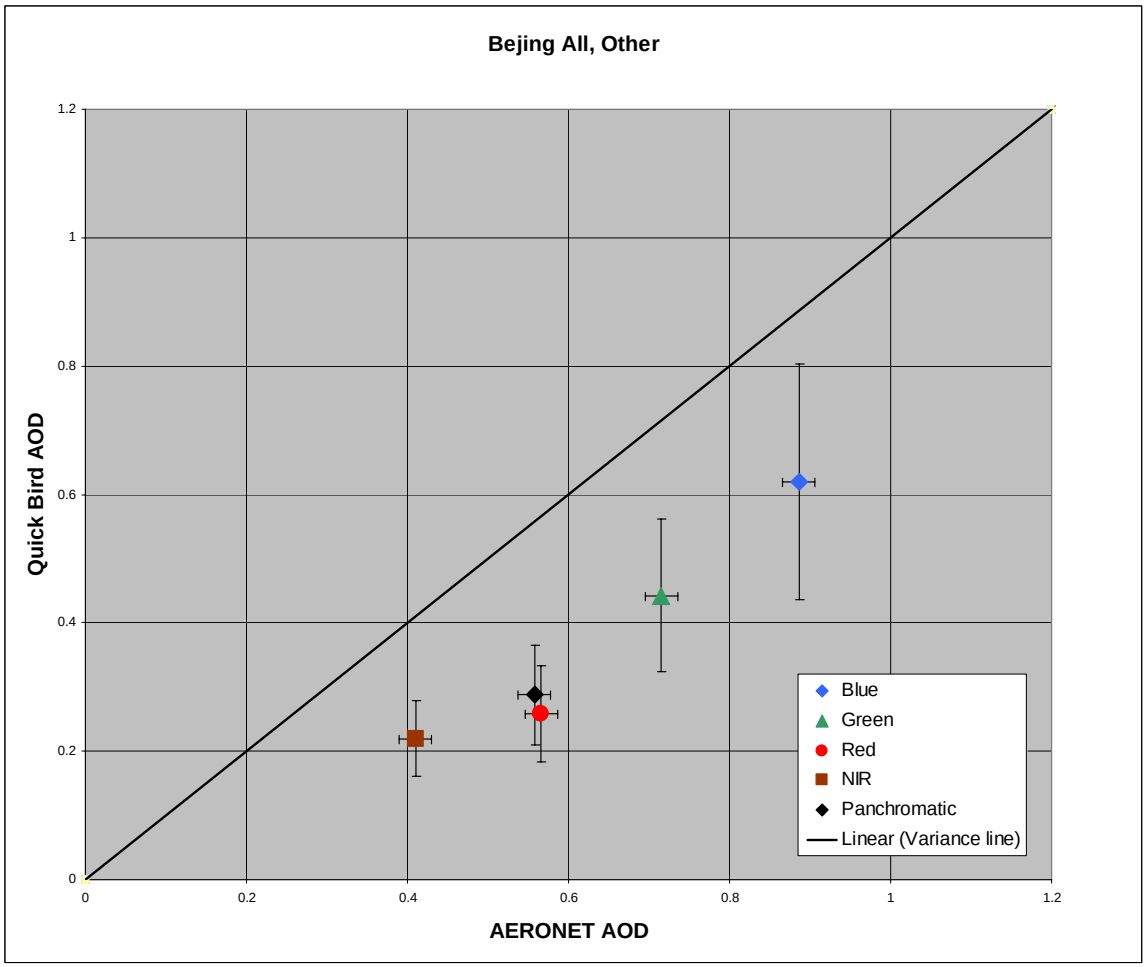

Figure 32. Comparison of QuickBird Shadow Method derived AOD with AERONET derived AOD for ROIs of all other surfaces and all shadow lengths. The vertical error bars indicated Shadow Method AOD standard deviation while the horizontal error bars indicate the uncertainty of the AERONET.

Table 24. Shadow Method AOD other surface. Shadow Method AOD results for ROIs of other surfaces and all shadow lengths.

Channel	Blue	Green	Red	NIR	Pan
Mean (all)	0.62	0.44	0.26	0.22	0.29
Standard Deviation	0.18	0.12	0.08	0.06	0.08

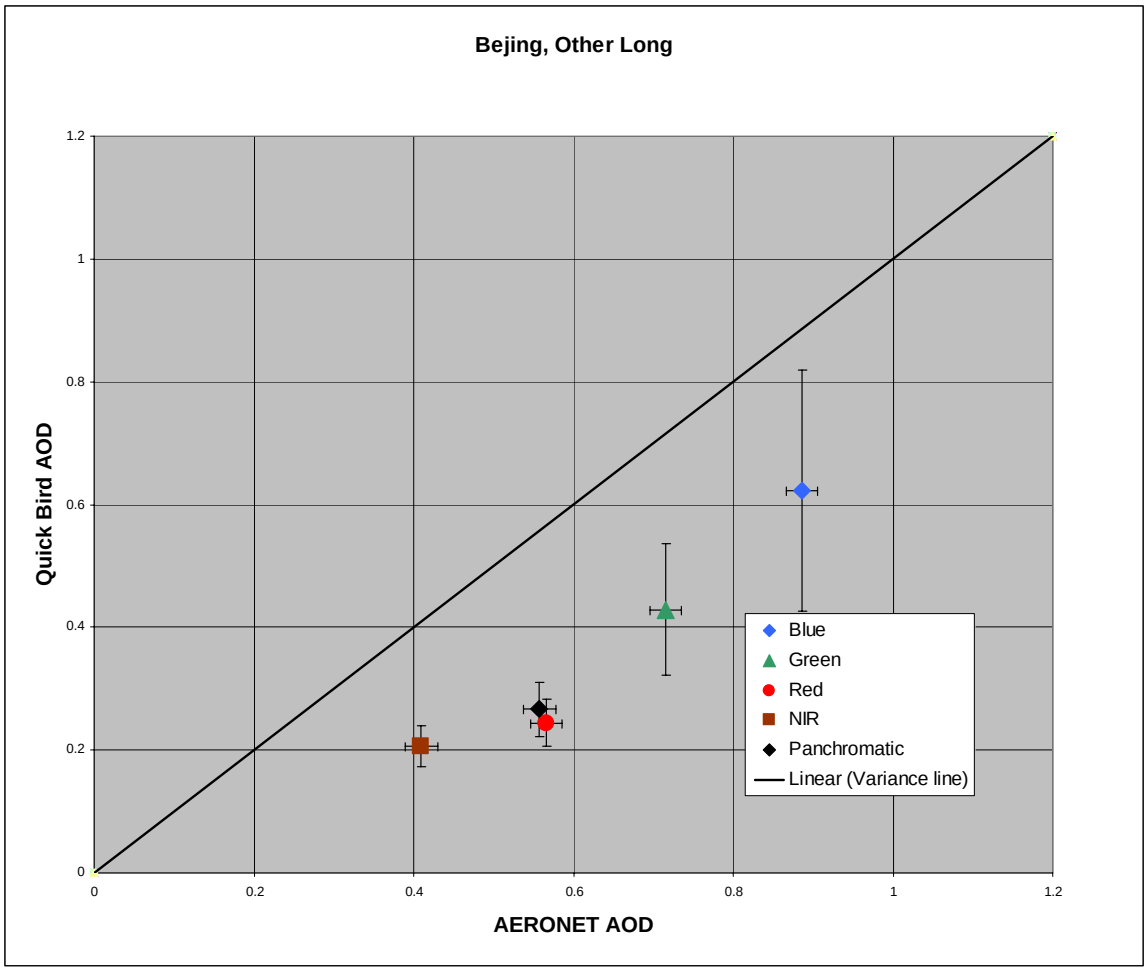

Figure 33. Comparison of QuickBird Shadow Method derived AOD with AERONET derived AOD for ROIs of other surfaces with long shadows. The vertical error bars indicated Shadow Method AOD standard deviation while the horizontal error bars indicate the uncertainty of the AERONET.

Table 25. Shadow Method AOD other surface long shadows. Shadow Method AOD results for ROIs of other surfaces and long shadows.

Channel	Blue	Green	Red	NIR	Pan
Mean (long)	0.62	0.43	0.24	0.21	0.27
Standard Deviation	0.20	0.11	0.04	0.03	0.04

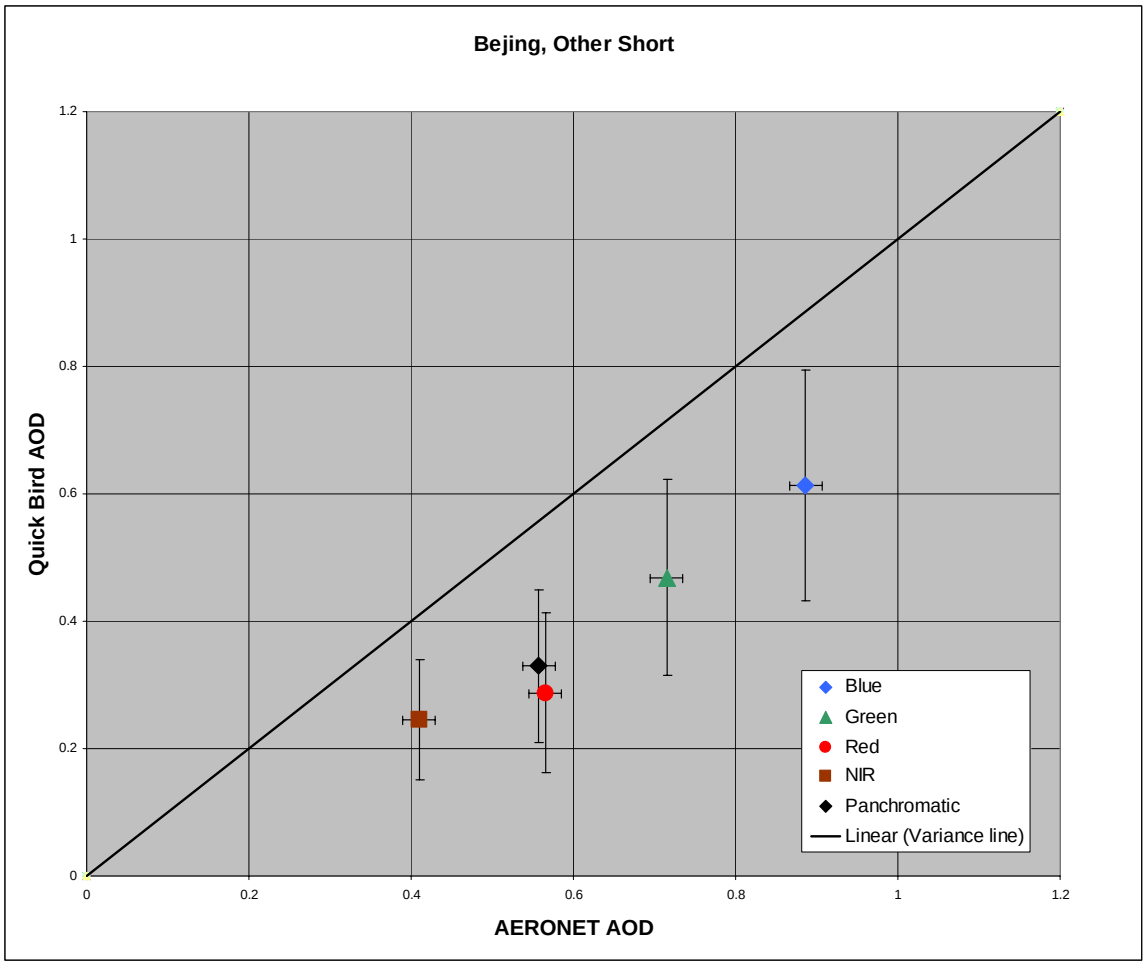

Figure 34. Comparison of QuickBird Shadow Method derived AOD with AERONET derived AOD for ROIs of other surfaces with short shadows. The vertical error bars indicated Shadow Method AOD standard deviation while the horizontal error bars indicate the uncertainty of the AERONET.

Table 26. Shadow Method AOD other surface with short shadows. Shadow Method AOD results for ROIs of other surfaces and short shadows.

Channel	Blue	Green	Red	NIR	Pan
Mean (short)	0.61	0.47	0.29	0.25	0.33
Standard Deviation	0.18	0.15	0.13	0.09	0.12

After reviewing the results from the "other" ROI cases, it is evident that the "other" ROIs demonstrate the same characteristics as the overall results. Implies retrieval technique is generally insensitive to surface type as long as the surface reflectance is relative high.

When comparing the results between the long and short shadows the calculations provide the expected higher calculated AODs for all but the blue channel. The results can bee seen in Table 27.

Table 27. Long vs. Short AOD analysis, Other ROIs. Analysis of the mean values for all other ROIs indicate that the Shadow Method calculations for short shadows tend to produce higher AODs than the long shadows with the exception of the blue channel. It must be noted that results are questionable with other ROIs due to a relatively small sample size.

Channel	Blue	Green	Red	NIR
Long shadows	0.62	0.43	0.24	0.21
Short shadows	0.61	0.47	0.29	0.25
Difference short-long	-0.01	0.04	0.04	0.04

5. Summary

When comparing the surface types, the most distinct observation is that all the surface types react remarkably the same with the exception of grass. Grass is the only low reflective surface type of those tested. It also is the one to most likely to be affected by Rayleigh scattering. The results for all the surface types are plotted together in Figure 35. Also, the inverse relationship between the wavelength of the channel and the standard deviation seen in the overall results holds true for all the surface types.

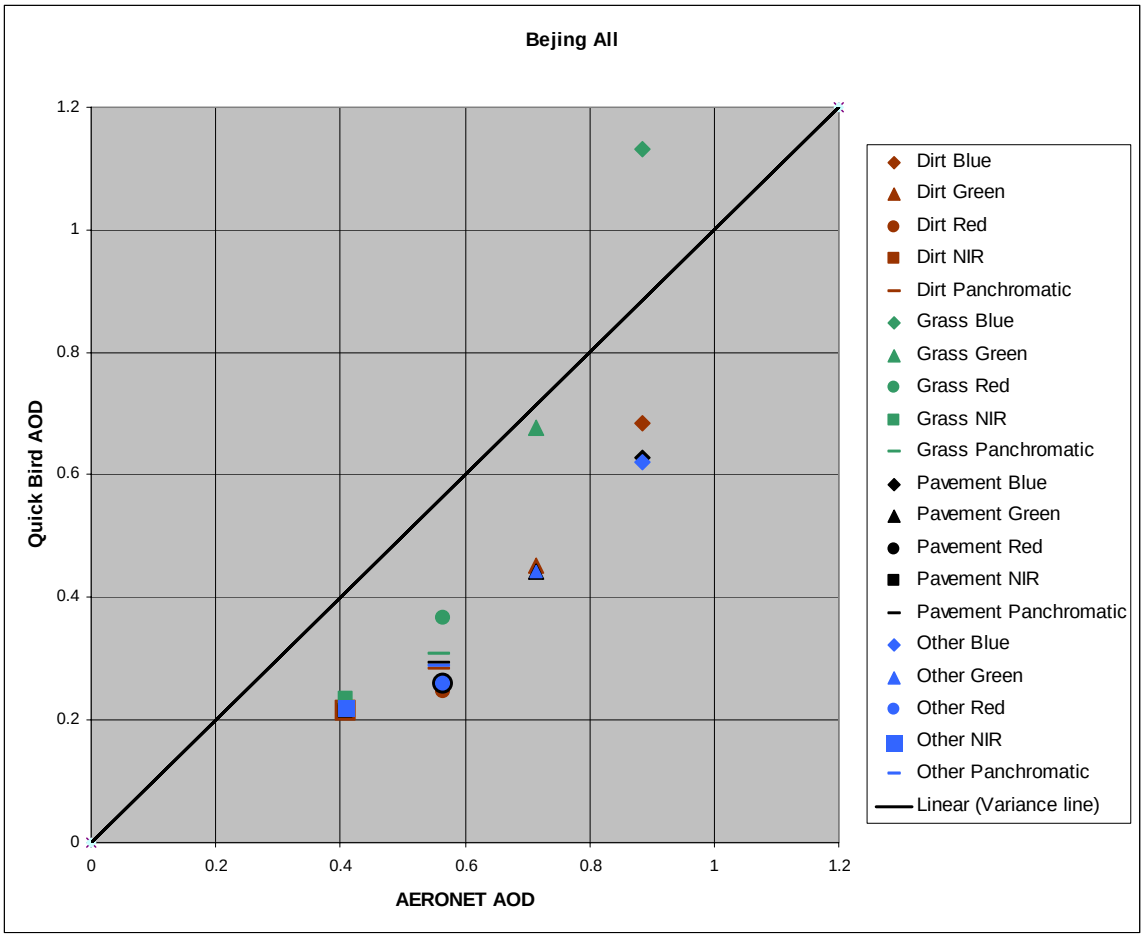

Figure 35. This figure shows the relationship between the different surface types relative to their QuickBird channel and derived AODs with respect to AERONET derived AODs. Note the strong agreement among all the surface types except for grass.

E. CHANNEL SPECIFIC ANALYSIS

The five QuickBird channels have a similar response for all the surface types. The error analysis, as seen in Table 28, shows that the blue channel has the least error compared to AERONET. The error increases as with the green channel and further increases with the red channel. The NIR on the other hand breaks this trend of increasing error with longer wavelengths and decreases its error. The panchromatic shows an error similar to the red channel. Also both the NIR and Panchromatic channels are extremely consistent across the surface types.

Table 28. Absolute AOD Error per Channel. This table shows the deviation of the mean Shadow Method derived AOD retrieval from the AERONET base line for each individual channel and surface type.

Channel	Blue	Green	Red	NIR	Pan
All	-0.10	-0.20	-0.27	-0.19	-0.26
Dirt	-0.17	-0.23	-0.29	-0.19	-0.26
Grass	-0.03	-0.17	-0.26	-0.19	-0.26
Pavement	-0.06	-0.18	-0.26	-0.19	-0.26
Other	-0.16	-0.22	-0.29	-0.19	-0.26

When looking at the standard deviations there is also variations observed as a function of wavelength. Across all the channels and all surface types the standard deviation increase with decreasing wavelength. This decrease is fairly substantial from the blue channel down to the NIR channel. The panchromatic channel also shows quite low standard deviations. Note the standard deviations for the dirt surface type are questionable due to the small sample size but they still show the same variations as a function of wavelength. These variations indicate that the longer the wavelength, the more consistent the AOD results will be. The break down of the standard deviations can be seen in Table 29.

Table 29. This table shows the standard deviation of the mean Shadow Method derived AOD retrievals. Note that as the wavelength increases that the standard deviation decreases leading to the conclusion that longer wavelengths provide more consistent results.

Channel	Blue	Green	Red	NIR	Pan
All	0.22	0.12	0.06	0.03	0.05
Dirt	0.11	0.08	0.07	0.03	0.05
Grass	0.34	0.09	0.10	0.04	0.04
Pavement	0.12	0.08	0.05	0.04	0.04
Other	0.18	0.12	0.08	0.06	0.08

F. SPATIAL ANLYSIS

When performing the Shadow Method AOD retrieval and comparing it to the AERONET results there is a potential for error based on the spatial properties of the sampled location. For example, one portion of a city may have a significant amount of

industrial pollution in the air while the AERONET ground truth site may be in a relatively clean part of the city. Or the AERONET site may be immediately down stream from a single point source of aerosols, thereby providing an unrepresentative assessment of the regional AOD environment. To explore this possibility, the data was analyzed by projecting the AOD values for each channel based on their latitude and longitude. Figures 36-39 provide this spatial representation of the Shadow Method AOD retrievals for the QuickBird blue, green, red, NIR, and panchromatic channels respectively. The colors indicate the level of AOD and can be used to identify variations in the aerosol distribution. No coherent areas of higher or lower concentrations are apparent to explain the variance in the results.

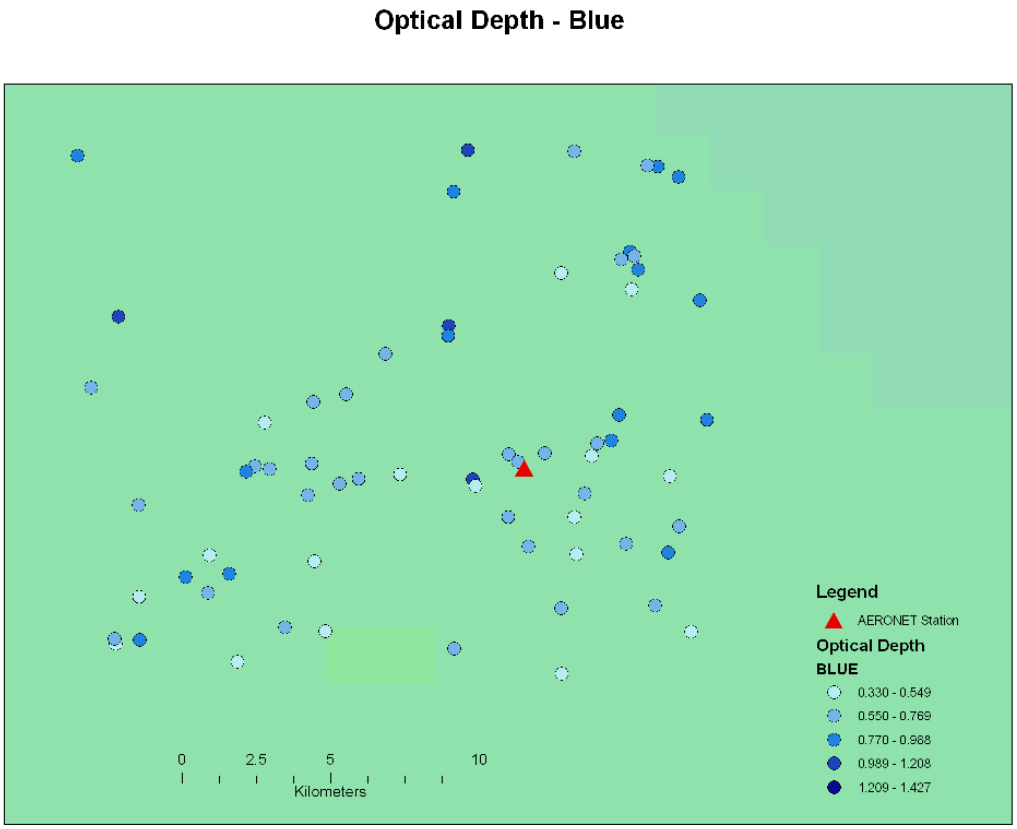

Figure 36. This figure contains the location and associated AOD values for the QuickBird blue channel from the AERONET station (red triangle) Guest, A. (2006).

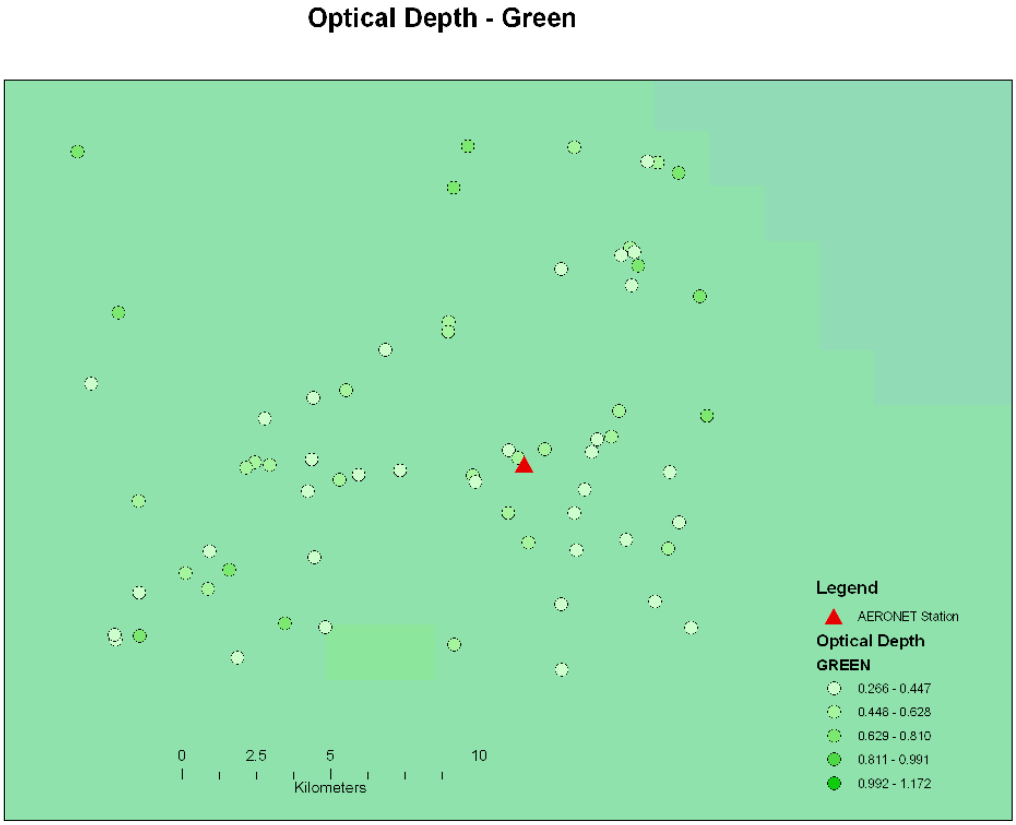

Figure 37. This figure contains the location and associated AOD values for the QuickBird green channel from the AERONET station (red triangle) Guest, A. (2006).

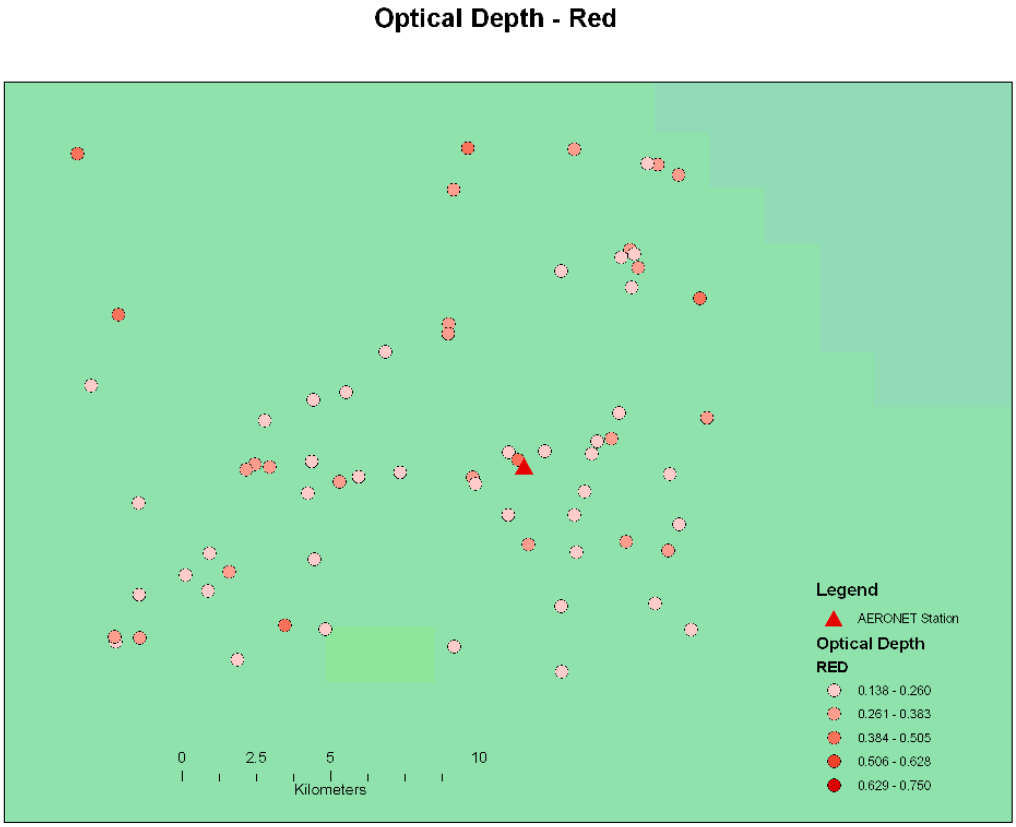

Figure 38. This figure contains the location and associated AOD values for the QuickBird red channel from the AERONET station (red triangle) Guest, A. (2006).

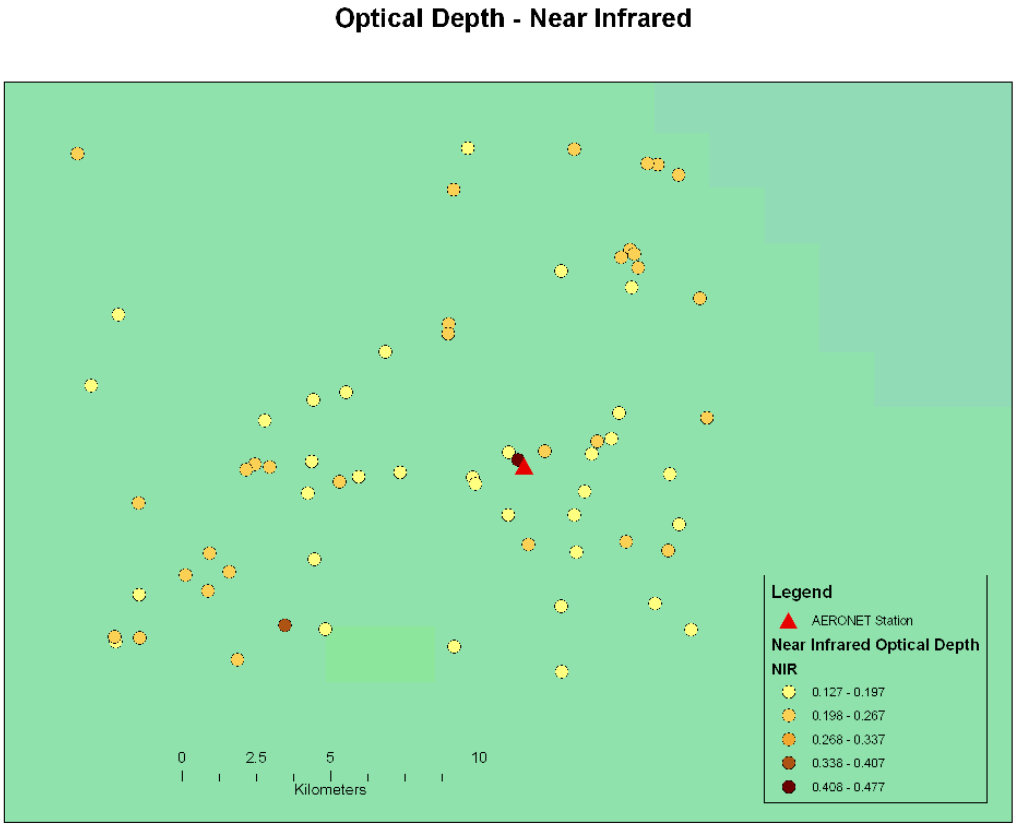

Figure 39. This figure contains the location and associated AOD values for the QuickBird NIR channel from the AERONET station (red triangle) Guest, A. (2006).

G. URBAN EFFECT

As described in Chapter III, the surrounding buildings were considered for possible impacts on the scenes for each specific ROI. Fifty-two cases were determined to have buildings capable of possible affects on the ROI scene and 24 cases were determined to be sufficiently far from other tall structures that there should be little to no effect on the scene. Table 30 shows the Shadow Method derived AODs for the overall average of all ROIs, ROIs containing surrounding buildings, and ROIs without surrounding buildings. A direct comparison can also be made with the AERONET derived AODs.

Table 30. Urban Effect Comparison. This table shows a comparison between all scenes, scenes containing surrounding buildings (urban effects), scenes without buildings, and AERONET derived AODs

Channel	Blue	Green	Red	NIR	Pan
AERONET derived AOD	0.89	0.72	0.57	0.41	0.56
All ROIs	0.79	0.52	0.29	0.22	0.30
ROIs containing buildings	0.78	0.53	0.30	0.22	0.31
ROIs with out buildings	0.82	0.50	0.29	0.22	0.28
Difference (bldgs-with out bldgs)	-0.04	0.03	0.01	0.00	0.03

After the scenes were broken down between those that contained structures in close proximity, they were further categorized by the apparent affects. Table 31 represents a sample set of 11 cases in which the surrounding buildings have sunlit faces facing the ROIs and how it compares to the mean scene with buildings in close proximity.

Table 31. Mean ROI with surrounding buildings AOD vs. ROIs with illuminated surrounding building faces. This table shows the difference between ROIs with surrounding buildings with sunlit faces in close proximity and all the ROIs containing buildings in close proximity.

Channel	Blue	Green	Red	NIR	Pan
ROIs containing buildings	0.78	0.53	0.30	0.22	0.31
ROIs w/ lit surronding buildings	0.86	0.58	0.31	0.24	0.32
Change	0.09	0.05	0.02	0.02	0.01

The opposite scenario where there are only buildings in close proximity with shaded faces near the ROIs are contained in Table 32 and represent a total set of 13 ROIs.

Table 32. Mean ROI with surrounding buildings AOD vs. ROIs with surrounding buildings with shaded faces. This table shows the difference between ROIs with surrounding buildings with shaded faces in close proximity and all the ROIs containing buildings in close proximity.

Channel	Blue	Green	Red	NIR	Pan
ROIs containing buildings	0.78	0.53	0.30	0.22	0.31
ROIs shaded surronding buildings	0.77	0.52	0.31	0.22	0.32
Change	-0.01	-0.01	0.01	0.00	0.01

The third scenario where there are buildings on at least three sides in close proximity with both shaded faces and sunlit faces near the ROIs are contained in Table 35 and represent a total set of 14 ROIs.

Table 33. Mean ROI with surrounding buildings AOD vs. ROIs with surrounding buildings on at least three sides. This table shows the difference between ROIs with surrounding buildings on at least three sides with both shaded faces and sunlit faces in close proximity and all the ROIs containing buildings in close proximity.

Channel	Blue	Green	Red	NIR	Pan
ROIs containing buildings	0.78	0.53	0.30	0.22	0.31
ROIs w surronding buildings on at	0.88	0.58	0.32	0.22	0.32
Change	0.10	0.06	0.02	0.00	0.01

Tables 31-33 do not show any specific trend to explain a shift of the AOD in one direction or another. In fact all three tables show little change or even an increase in the AOD which is counter to the low biases that have been observed. When the rest of the ROIs that have surrounding buildings, and do not fall into any of the above three categories, are examined, the only trends that are observed is that they typically have both buildings with sunlit faces and shaded faces, but not on three or more sides of the ROI, and they tend to have pavement as their primary surface type. This suggests that specular reflection may be a factor in the AODs observed.

V. CONCLUSION

Overall the results obtained from this study are promising. They show a correlation that was not previously seen in the limited urban study performed by Vincent (2006). The reasons for this may be due to a larger sample size per case or possibly more controlled ROI selection. Regardless this study has shown a consistency in the results to indicate that the Shadow Method is viable in an urban environment.

A. AEROSOL OPTICAL DEPTH RESULTS

1. Low Bias

The first and most obvious observation that stands out is the strong low bias seen in the AOD results. These biases are seen across all surface types and all channels with the exception of the blue and green channels over a grass surface.

These biases are larger than those shown in Vincent (2006). Vincent's results in a desert environment were closer to the AERONET ground truth results. However, his attempts at using the Shadow Method in an urban environment were uncorrelated with AERONET derived AOD results and is one of the reasons that this thesis is being performed.

Although the reasons for the biases were not captured in the scope of this thesis, there are three possibilities that should be explored. The first possibility is an unrepresentative aerosol model. The Shadow Method program used a single scatter albedo value of 0.95 (Vincent, 2006). Dombrock (2007) performed a limited sensitivity test with respect to the single scatter albedo. He changed the value from 0.95 to 0.88. This change resulted in an increase of the AOD in the blue, green, and red channels of about .04 and an increase in the NIR channel of about .01. Metar observations taken at the time of the satellite imagery indicate 2.5 miles of visibility with smoke reported as the obscuring phenomena. It seems reasonable that a correction in the aerosol model has the

potential to account for at least some of the bias. Further study with respect to the aerosol model was not undertaken in the scope of this thesis but is an avenue that should be explored.

The second possibility for the low bias is that this study took place in an urban environment. The urban effect can potentially affect a scene in two ways. The first way of affecting a sample area is for buildings to block the celestial dome. In other words, near by buildings act to block the view of the sky from the point where the sample is being taken. This blockage of the sky prevents scattered light from atmospheric aerosols from making it to both the shaded and unshaded regions of the sample area. It is assumed that in most cases that the shadow sampled is typically closer to the shadow casting structure than the unshaded sample region and therefore has a greater blockage of the sky. If this is true the shadow area will have less light scattered into it acting to make the shadow darker. The darker shadow acts to increase the difference between the shaded and unshaded regions of the sample, causing the AOD to appear lower than reality. The second way involves surrounding buildings acting as reflectors of radiance into our sample area. It is not uncommon for nearby buildings to be illuminated, and some buildings can be highly reflective. They then have the potential to add radiance to the area being sampled. In this particular case it is usually assumed that the unshaded portion of the sample area is closer to surrounding buildings than the shaded. It also seems reasonable that the areas closer to a reflecting building will receive more radiance than areas further away assuming lambertian reflectance. If this is the case the difference between the shaded region and unshaded region will increase, resulting in a decrease in the calculated AOD.

The third possibility that should be explored is not urban specific. In all of the cases lambertian reflectance is assumed. Some surfaces may act more as a specular reflector. The abundance of pavement in an urban scene makes this characteristic potentially significant. With specular reflection, the solar zenith angle, sensor view angle, and even the orientation of the surface become important and have the potential of providing radiance values dependent on the combination of these three factors.

2. Long Shadow vs. Short Shadow Analysis

The sampling process or the definition of the ROIs can play a critical role in the accuracy of the AOD calculation process. Poorly chosen ROIs can introduce unrepresentative pixels that skew the data in one direction or another. During the ROI sampling process for this study, great care was taken to insure that the sample areas were as clean as possible and free from contamination by unrepresentative pixels. Multispectral images were cross referenced with the higher resolution panchromatic images to screen out sub pixel contamination. It is believed that for the reasons discussed in Chapter IV that short shadows will produce an AOD result higher than cases where there is a long shadow.

Though the increased AOD for short shadow length hypothesis holds up under inspection for the mean of all the ROIs it does not necessarily hold true when comparisons are made while looking at specific surface types. The dirt surface shows mixed results. It is difficult to draw any hard conclusions with the dirt cases due to the relatively small sample size. Looking at all the cases containing grass good agreement across all the channels is observed. Pavement on the other hand shows the exact opposite. All the short shadows actually show a decrease in the AOD when looking at short shadows as compared to long shadows. This is as of yet unexplained. One possible cause of this phenomena is the possibility that there may be an increase in specular reflection of pavement may overwhelm edge effect. The “other” surface type tends to agree with this theory except for the blue channel. It should be noted that the “other” surface type category also has a relatively small sample size.

Standard deviation, which is one of the indicators of uncertainty, is also affected when a comparison between long shadows and short shadows is made. It is expected that short shadows will have a greater standard deviation due to the variability caused by edge effects. This is observed in the short shadow cases and indicates that their results are less consistent.

3. Surface Type AOD Analysis

The surface type analysis shows that, of the four surface types tested, three show strong agreement. The deviation observed with grass is believed to be caused by either the poor ability of the Shadow Method program to properly estimate the surface reflectance of a weakly reflective surface, the impacts of Rayleigh scattering, or both.

4. Channel Specific Analysis

The five QuickBird channels have a very similar response for all the surface types. The blue channel shows the least amount of error with a slight increase in error as wavelength is increased up to the red channel. The panchromatic results are typically very close to the results for the red channel. Also, as wavelength is increased the AOD results from across the surface types become more consistent. In addition, in every case the standard deviation decreases with wavelength. This decrease is fairly substantial from the blue channel down to the NIR channel. The panchromatic channel also has a low standard deviation. In other words the longer the wavelength is the more consistent the results will be. It is believed that the decreasing standard deviation is due to the diminishing impact or Rayleigh scattering.

Based on these observations one should not assume that the shorter wavelengths are more accurate. These results do not take into account the, as of yet, undetermined factors leading to the low bias. Consistency should also be a consideration. Once the factors are determined that lead to the biases, the channels with the longer wavelengths and the panchromatic channel would be expected to provide more consistent results.

B. FUTURE RESEARCH

1. Determination of Low Bias

The first study that needs to be done is the determination of the root cause of the consistent low bias seen throughout the channels. The first step in this is to do more case studies in a similar environment to determine if there is something specific to this day and scene that is the cause of the low bias.

The second element to study should be to explore the aerosol model. Dombrock (2007) showed that a change in the single scatter albedo can play a factor in the results of the Shadow Method calculations. The asymmetry factor may also play a role. Though the method may not be sensitive in most cases to the aerosol model; there may be certain environments where the aerosol model may have a larger influence.

The third area to focus on is how the urban environment affects the radiative environment of the scene. A controlled study is recommended. A site would need to be selected where the shadow casting structures can be manipulated so their exact affects, locations, and orientations can be measured over different surface types. It would also be advisable to test how the reflectance of the shadow casters interacts with the scene.

Another aspect that should be considered is the possible affect that specular reflection can have on the retrieved AODs. This can be done by constructing a scene with a surface that has multiple surface orientations that fall within a single shadow, or the construction of multiple scenes with identical shadow producers casting shadows over surfaces with different orientations. This may be done using aerial photography or even the use of handheld photography.

2. Use of the Shadow Method with Other Platforms

The next area that should be explored is the use of the Shadow Method with platforms other than satellite imagery. This study showed that panchromatic imagery proved to be quite consistent. Other platforms such as UAVs or other intelligence gathering means could provide a timelier means of gathering this information for those that need to use it operationally.

THIS PAGE INTENTIONALLY LEFT BLANK

LIST OF REFERENCES

Ahrens, C. Donald 1994: Meteorology Today an Introduction to Weather, Climate, and the Environment. 461-469, 560.

Boubel, W. Richard, and Fox, L. Donald, and Turner, D. Bruce, and Stern, Arthur C. 1994: Fundamentals of Air Pollution. 72-79, 250, 262-267, 275-287, 291-294.

DigitalGlobe, cited February 2007: QuickBird Specifications. [Available at http://www.digitalglobe.com/about/quickbird.html].

Dombrock, R., 2007: Automating Shadow Method for AOD Retrieval. M.S. thesis, Department of Meteorology, Naval Postgraduate School, CA, 59 pp.

Dombrock, R., 2007: Personal Communication.

Fraser, R. S., Y. J. Kaufman, and R. L. Mahoney, 1984: Satellite measurements of aerosol mass and transport. *Atmos. Environ.*, **18**, 2577-2584.

Frolich, C., and G.E. Shaw, 1980: New determination of Rayleigh scattering in the terrestrial atmosphere. *Appl. Opt.*, **19**, 1773-1775.

Goddard Space Flight Center (GSFC), cited February 2007: Aerosol robotic network (AERONET). [Available on line at http://aeronet.gsfc.nasa.gov/].

Goddard Space Flight Center (GSFC), cited March 2007: MODIS Web. [Available on line at http://modis.gsfc.nasa.gov/].

Guest, A., 2006: Personal Communication.

Hsu, N. C., S. C. Tsay, M. D. King, and J. R. Herman, 2004: Aerosol properties over bright-reflecting source regions. *IEEE Trans. Geosci. Remote Sensing*, **42**, 557-569.

ITT, cited February 2007: [Available on line at http://www.ittvis.com/envi/]
The ATSR Project, cited 2007: [Available on line at http://www.atsr.rl.ac.uk/demo/demo/demo/index.html].

Jet Propulsion Laboratory (JPL), cited February 2007: Multi-angle Imaging Spectro Radiometer (MISR). [Available on line at http://www-misr.jpl.nasa.gov/mission/iangles.html].

Kaufman, Y. J., and J. H. Joseph, 1982: Determination of surface albedos and aerosol extinction characteristics from satellite imagery. *J. Geophys. Res.*, **87**, 1287-1299.

Kaufman, Y. J. and C. Sendra, 1988: Algorithm for automatic atmospheric corrections to visible and near-IR satellite imagery. *Int. J. Remote Sens.*, **9**, 1357-1381.

Kaufman, Y. J., D. Tanre, L. A. Remer, E. F. Vermote, A. Chu, and B. N. Holben, 1997: Operational remote sensing of tropospheric aerosol over land from EOS moderate resolution imaging spectroradiometer. *J. Geophys. Res.*, **102**, 17051-17067.

Martonchik, J. V., Diner, D. J., Kahn, R., and Gaitley ,B., 2004: Comparison of MISR and AERONET aerosol optical depths over desert sites. *J Geophys. Res.*, **31**, L16102, 1-4.

Russell, P. B., J. M. Livingston, E. G. Dutton, 1993: Pinatubo and pre-Pinatubo optical depth spectra: Mauna Loa measurements, comparisons, inferred particle size distributions, radiative effects, and relationship to lidar data. *J. Geophys. Res.*, **98**, 22969-22985.

Tanre, D., P. Y. Deschamps, C. Devaux, and M. Herman, 1988: Estimation of Saharan aerosol optical thickness from blurring effects in Thematic Mapper data. *J. Geophys. Res.*, **93**, 15955-15964.

The ATSR Project, cited February 2007: Along Track Scanning Radiometer (ATSR). [Available on line at http://www.atsr.rl.ac.uk/].

Veefkind, J. P., deLeeuw, G., and Durkee, P.A., 1998: Retrieval of Aerosol Optical Depth over Land using two-angle view Satellite Radiometry during TARFOX, *Geophys Res. Lett.*, 25 3135-3138.

Vincent, D. A., 2006: Aerosol optical depth retrievals from high-resolution commercial satellite imagery over areas of high surface reflectance. PhD Dissertation, Department of Meteorology, Naval Postgraduate School, CA, 5-10, 143-152 pp.

Wehrli, C., 1985: Extraterrestrial Solar Spectrum – Publ. 615. Physical Meteorological Observatory and World Radiation Center, Davos Dorf, Switzerland.

THIS PAGE INTENTIONALLY LEFT BLANK

INITIAL DISTRIBUTION LIST

1. Defense Technical Information Center
   Ft. Belvoir, Virginia

2. Dudley Knox Library
   Naval Postgraduate School
   Monterey, California

3. Professor Philip A. Durkee (Code MR/DE)
   Department of Meteorology
   Naval Postgraduate School
   Monterey, California

4. Professor Carlisle H. Wash (Code MR/WX)
   Department of Meteorology
   Naval Postgraduate School
   Monterey, California

5. Capt Jack R. Evans
   Department of Meteorology
   Naval Postgraduate School
   Monterey, California